PHYSICAL REVIEW D VOLUME 18, NUMBER 4 15 AUGUST 1978

High-speed black-hole encounters and gravitational radiation

P. D. D'Eath
Department of Applied Mathematics and Theoretical Physics, Silver Street, Cambridge, England
(Received 15 March 1977)

Encounters between black holes are considered in the limit that the approach velocity tends to the speed of light. At high speeds, the incoming gravitational fields are concentrated in two plane-fronted shock regions, which become distorted and deflected as they pass through each other. The structure of the resulting curved shocks is analyzed in some detail, using perturbation methods. This leads to calculations of the gravitational radiation emitted near the forward and backward directions. These methods can be applied when the impact parameter is comparable to $Gc^{-2}M\gamma^2$, where M is a typical black-hole mass and γ is a typical Lorentz factor (measured in a center-of-mass frame) of an incoming black hole. Then the radiation carries power/solid angle of the characteristic strong-field magnitude c^5G^{-1} within two beams occupying a solid angle of order γ^{-2}. But the methods are still valid when the black holes undergo a collision or close encounter, where the impact parameter is comparable to $Gc^{-2}M\gamma$. In this case the radiation is apparently not beamed, and the calculations describe detailed structure in the radiation pattern close to the forward and backward directions. The analytic expressions for strong-field gravitational radiation indicate that a significant fraction of the collision energy can be radiated as gravitational waves.

I. INTRODUCTION

Although there have been many calculations of gravitational wave generation within the context of general relativity, little is known about truly strong-field radiation which originates in highly nonlinear interaction processes. In particular, no exact solutions of the field equations have yet been found which are asymptotically flat and contain gravitational radiation. Radiation calculations are usually carried out by perturbation methods, with the result that most analytic expressions for waves emitted from local systems are valid only in the limit that the strength of the radiation tends to zero. For example, the radiative field of a small body of mass m moving in a background spacetime scales like m as $m \to 0$, while in a post-Newtonian treatment of a bound system of masses moving with low velocities of order ϵ, the radiative part of the metric scales down rapidly as ϵ^5. This can be expressed more physically by saying that most perturbation approaches are only useful for calculating radiation fields when the power involved is much less than $c^5/G \simeq 3.6 \times 10^{59}$ erg/sec, the characteristic power associated with fully nonlinear gravitational interactions.[1]

It is then important to try to extend the range of perturbation theory as far as possible, in order to obtain more information about the two types of processes which can lead to fully nonlinear radiation, namely nonspherical stellar collapse and collisions between strongly relativistic bodies with comparable masses or energies. We shall see in this paper that perturbation methods can actually be used to make analytic statements about strong-field gravitational radiation produced by collisions of black holes at velocities close to the speed of light.

There are two reasons for considering the black-hole collision problem in the limit that the relative velocity tends to c, rather than a situation where the two black holes approach each other with only moderate velocities at early times. First, there is the possibility that the form of the spacetime metric produced by the collision simplifies in the high-speed limit. The metrics due to collisions at precisely the speed of light will be special boundary cases among the family of all black-hole collision metrics, and may well be more tractable analytically. Any attempts to find exact solutions of the vacuum Einstein equations, describing black-hole collisions, should then start with the simplest of these limiting spacetimes, in which the impact parameter is zero and the geometry axisymmetric.

Second, some geometrical simplifications also take place for the high-speed collision. The gravitational field of an incoming black hole with mass M_1 and energy $\mu = M_1\gamma_1$ becomes concentrated owing to special-relativistic effects in a shock wave close to a null plane in the surrounding nearly Minkowskian spacetime, when γ_1 is large; the shock will be accurately approximated by a certain type of impulsive plane-fronted wave[2,3] with strength proportional to μ, provided that we ignore the detailed structure near the plane. Then suppose that we work in a center-of-mass frame and examine the collision of two black holes with comparable masses M_1 and M_2 moving in opposite directions with high velocities, such that the incoming energies $M_1\gamma_1$ and $M_2\gamma_2$ are both equal to μ. In this case we can divide the spacetime up

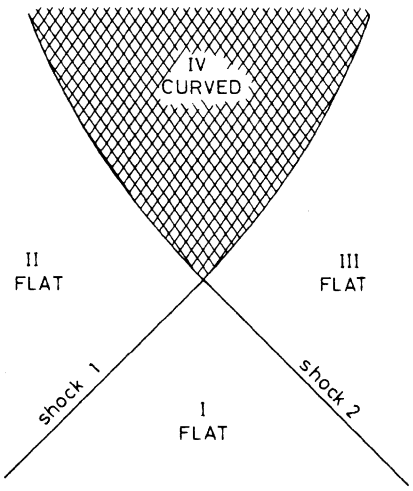

FIG. 1. Schematic spacetime diagram for a collision of two black holes approaching at the speed of light. Before the collision, the spacetime curvature due to black hole 1 resides on a null hyperplane, denoted by shock 1, which separates two regions I and II of flat spacetime. Similarly there is a null shock 2 produced by black hole 2, which separates region I from another flat region III. At the collision, the null generators of each shock acquire shear and begin to converge; thereafter the shock surfaces are curved. Spacetime curvature develops in the region IV to the future of the collision.

into four basic regions (see Fig. 1), if we again ignore the detailed structure of the gravitational field near the shocks. Ahead of both incoming shocks the spacetime will be nearly flat (region I). Behind shock 1 due to the black hole M_1 there will be another nearly flat region II, where the geometry has not yet been disturbed by information propagating from the collision. Shock 1 will be effectively a null surface in the subset of Minkowski space formed by the union of regions I and II, and can be given say by the relation $z-t=0$ in Minkowskian coordinates. There will be a similar nearly flat region III behind shock 2, which will be given by the relation $z+t=0$ in Minkowskian coordinates defined on the union of regions I and III, and which has the same strength as shock 1. Regions II and III will also be bounded by shocks which have emanated from the collision. These shocks will lie on curved surfaces when viewed from the Minkowskian regions to their immediate past, and are found by following the null geodesic generators of the incoming plane shocks through the spacelike two-surface on which the incoming shocks meet (the collision two-surface). In fact, the curved shocks will constitute the boundary of the future of the collision two-surface, and form an achronal surface[4] (containing no two points with timelike separation) which is almost everywhere null. The generators of shock 1, say, will have acquired some shear at the collision with shock 2, and will thereafter be both shearing and converging. Behind both curved shocks 1 and 2 there will be a strongly curved interaction zone (region IV) where the gravitational field behaves in a highly nonlinear manner. The union of curved shocks 1 and 2 will be a characteristic initial surface for the solution of the vacuum Einstein equations in region IV.

This geometrical framework has been exploited by Penrose,[5] who has found apparent horizons (compact spacelike two-surfaces such that the convergence of the outgoing normal family of null geodesics is zero) on the union of the incoming plane null surfaces, for a range of values of the quantity (impact parameter)/μ. This information can then be used to bound the amount of radiation arriving at future null infinity due to the collision, if one makes the "cosmic censorship hypothesis," which claims that any singularities formed during the evolution of reasonable initial data will be hidden behind an event horizon. Under this assumption, the areas of the apparent horizons found by Penrose provide lower bounds for the areas of black holes left as final products of the collision. Energy conservation then limits the strength of the radiation; for example, Penrose has shown in this way that the energy radiated in the axisymmetric speed-of-light collision must be less than 50% of the original 2μ, under the "cosmic censorship hypothesis." Conversely, if too much energy is radiated away in a collision, then the hypothesis must be false.

The collision at precisely the speed of light has various mildly undesirable features, caused by the infinite Lorentz contraction of the incoming states, which pushes all the curvature into δ functions on the null planes. This implies that the spacetime is, strictly speaking, not asymptotically flat in the past, and also that the curvature falls off only as r^{-2} instead of the usual r^{-3} at large spacelike distances. Further, we shall see that the spacetime is not quite asymptotically flat at future null infinity, owing to some (fairly harmless) singularities in the radiation field. To avoid these difficulties, we prefer in this paper to keep γ_1 and γ_2 large but finite, and to consider limiting properties of the spacetimes as $\gamma_1, \gamma_2 \to \infty$ with M_1, M_2 varying so that $M_1\gamma_1 = M_2\gamma_2 = \mu$ is fixed; then the singular features of the $\gamma = \infty$ collision will be smeared out. We emphasize that the energy μ is to be regarded as a quantity of $O(1)$ in perturbation theory. More precisely, we shall consider one-parameter families of spacetimes containing colliding black holes of comparable mass, where we also fix the ratio M_1/M_2 as $\gamma_1, \gamma_2 \to \infty$. To give

a complete prescription for a one-parameter family, the scaling of the impact parameter as $\gamma \to \infty$ must further be specified. Then we shall examine the behavior of the gravitational field in the various qualitatively different regions of spacetime, described by different asymptotic expansions.

The various asymptotic expansions are needed to allow for the different length and time scales characteristic of the gravitational field. For example, the incoming plane shocks 1, 2 and the curved shocks 1, 2 have detailed structure on length scales of $O(\gamma^{-1})$ measured through the shock, due to the special-relativistic contraction, while the structure only varies over scales of $O(1)$ in spacetime directions parallel to the shock. More complicated behavior, with rapid variations in two or three spacetime directions, occurs near the collision two-surface where the shocks meet, and in two caustic regions on the curved shocks, where one shock has been almost infinitely focused by the other. Another type of behavior occurs in the interaction zone (region IV), where the gravitational field will be slightly perturbed away from the exact $\gamma = \infty$ metric, since γ_1, γ_2 are not quite infinite, but where there is no rapid variation in preferred directions. A separate perturbation expansion must be set up for each qualitatively different region, adapted to these characteristic length and time scales. One expects that the expansions holding in adjacent regions of spacetime, such as the curved shock 1 and the interaction region IV, match smoothly onto each other; thus boundary conditions on one asymptotic expansion are provided by all the adjacent expansions. By proceeding in this way we shall be able to obtain some analytic information about radiation in the strong-field region IV without knowledge of the $\gamma = \infty$ interaction metric. This will be found by matching from expansions which describe the evolution of the curved shocks at late times out in the far field; we can in fact describe the radiation heading out at angles of $O(\gamma^{-1})$ from the initial collision direction, while remaining within the far-field curved shocks.

We should also mention another approach to radiation calculations for high-speed encounters, due to Curtis.[6] In this approach one considers only the collision of shock waves at precisely the speed of light. Curtis has calculated the results of scattering a linearized plane-fronted wave against a fully nonlinear plane-fronted wave, and of scattering two weak plane-fronted waves off each other. But note that the statements in perturbation theory resulting from these calculations can be rephrased as statements about behavior in certain regions of the fully nonlinear spacetime produced by the collision of two shocks with equal strengths μ, for one can always arrange that two incoming null particles have equal energies, by performing a Lorentz boost. Then a transformation $g_{ab} \to N^2 g_{ab}$ with a constant conformal factor N^2 will scale up the energies by a factor N, without disturbing the vacuum Einstein equtions. In particular, this implies that Curtis's calculation of the scattering of a weak shock on a strong shock should relate to the radiation calculations of this paper, since the radiation which he finds can be reinterpreted as radiation close to the direction of motion in a center-of-mass nonlinear collision.

Although we shall always describe our perturbation schemes as representing collisions or encounters between high-speed nonrotating black holes, most of the statements will be valid for interactions between any pair of bodies with comparable masses M_1, M_2 at large γ_1, γ_2, such that $M_1\gamma_1 \gg R_1$, $M_2\gamma_2 \gg R_2$, where R_1, R_2 are typical proper radii of the bodies. This occurs because the metric is generated predominantly by the collision of the boosted Coulomb fields of the bodies, out at distances of order μ or further from their centers. We only choose to refer to interactions between bodies which are initially Schwarzschild black holes because of the need to specify all the spacetimes in the one-parameter families with $\gamma_1, \gamma_2 \to \infty$, used in the perturbation theory; the choice of incoming Schwarzschild states fixes a one-parameter family uniquely, once we have decided on the scaling of the impact parameter.

We will start in Sec. II by describing the geometry of an isolated Schwarzschild black hole which moves at high speed, considering both the detailed shock structure for large γ and the impulsive $\gamma = \infty$ shock. In Secs. III, IV, and V we restrict attention to the axisymmetric collision with zero impact parameter. In Sec. III we show how to follow the evolution of the detailed shock structure through the collision region and in the region where the shock surface is curved, at distances of $O(1)$ from the axis; the curved shock evolution is governed by geometrical optics, with the shock strength obeying an ordinary differential equation along the shock generators. The strength of each curved shock appears to grow indefinitely as we approach the caustic region on the axis, mentioned previously. In fact, some qualitatively new behavior takes over at distances of $O(\gamma^{-1})$ from the caustic region, in which the gravitational field becomes wavelike and a singularity can be averted. This self-interaction of the shock is of interest in its own right, and is described in Sec. IV. The calculation of radiation at angles of $O(\gamma^{-1})$ from the axis is carried out in Sec. V. It requires the description

of the curved shock evolution at large distances of $O(\gamma)$ away from the axis, at late times of $O(\gamma^2)$ after the collision; the shock evolution is qualitatively different from that described in Sec. III at distances of $O(1)$ away from the axis. In Sec. V we find the dominant radiation field analytically, close to the axis, and present numerical results. Similar methods can also be used for collisions and encounters with nonzero impact parameter. In particular, we describe in Sec. VI the regime where the impact parameter scales linearly with γ, and hence is of order γ^2 (mass), since we regard the energy μ as a quantity of $O(1)$. The black holes then only deflect each other slightly, and the radiation generated is strongly beamed near the direction of motion. With this scaling of the impact parameter, the radiation in the beam with half-angle of $O(\gamma^{-1})$ still has the strength characteristic of fully nonlinear interactions in general relativity. These calculations describe encounters which are much closer and produce much more radiation than those amenable to the usual flat-space perturbation methods for large γ; only when we let the impact parameter become much larger than γ^2(mass) do we find a radiation field proportional to M_1M_2, as in the standard "fast-motion" approaches. Finally in Sec. VII we summarize the various results.

II. THE INCOMING STATES

Suppose we take the Schwarzschild metric with mass M in isotropic coordinates,

$$ds^2 = -\left(\frac{1-M/2\bar{r}}{1+M/2\bar{r}}\right)^2 dt^2 + \left(1+\frac{M}{2\bar{r}}\right)^4 [d\bar{r}^2 + \bar{r}^2(d\theta^2 + \sin^2\theta d\phi^2)], \tag{2.1}$$

and make a coordinate transformation such that the black hole moves with a velocity $\beta = (1-\gamma^{-2})^{1/2}$ close to the speed of light, which is 1 in our units. We write the energy $M\gamma = \mu$. Then we consider the one-parameter family of such spacetimes found by letting $\gamma \to \infty$ with μ fixed. Aichelburg and Sexl[2] have shown that the metric approaches a limit, which can be put in the form

$$ds^2 = du\,dv + dx^2 + dy^2 - 4\mu \ln(x^2+y^2)\delta(u)du^2, \tag{2.2}$$

where $u = z+t$, $v = z-t$ and the motion is in the negative z direction.

It is clear from this form that the limiting metric is a special case of an axisymmetric plane-fronted wave[3] lying between two regions of Minkowski space. The detailed structure of the shock and the black-hole property have been lost by taking the limit $\gamma \to \infty$; the only length scale in the metric is now μ rather than M. Moreover, the infinite Lorentz boosting has changed the algebraic type of the Weyl tensor from type D for the Schwarzschild solution to type N for the limiting metric (2.2). To calculate the curvature, it is best to make a discontinuous coordinate transformation which puts the metric in a C^0 form, eliminating the δ function in Eq. (2.2). A suitable transformation is

$$\begin{aligned} x &= \hat{x} + 4\mu\,\hat{u}\theta(\hat{u})\hat{x}/(\hat{x}^2+\hat{y}^2), \\ y &= \hat{y} + 4\mu\hat{u}\theta(\hat{u})\hat{y}/(\hat{x}^2+\hat{y}^2), \\ v &= \hat{v} + 4\mu\,\theta(\hat{u})\ln(\hat{x}^2+\hat{y}^2) \\ &\quad -16\mu^2\hat{u}\theta(\hat{u})/(\hat{x}^2+\hat{y}^2), \\ u &= \hat{u}, \end{aligned} \tag{2.3}$$

where $\theta(\hat{u})$ is the Heaviside function. If we then write

$$\hat{x} = \hat{\rho}\cos\phi, \quad \hat{y} = \hat{\rho}\sin\phi, \tag{2.4}$$

the metric becomes

$$ds^2 = d\hat{u}d\hat{v} + [1 - 4\mu\hat{u}\theta(\hat{u})/\hat{\rho}^2]^2 d\hat{\rho}^2 + \hat{\rho}^2[1+4\mu\hat{u}\theta(\hat{u})/\hat{\rho}^2]^2 d\phi^2. \tag{2.5}$$

In these coordinates the metric only has a discontinuity in its first derivative at the shock surface $\{\hat{u}=0\}$, but there is the disadvantage that the Minkowskian form in $\{\hat{u}>0\}$ behind the shock has been lost. The only nonzero components of the Riemann tensor are

$$\begin{aligned} R_{\hat{x}\hat{u}\hat{x}\hat{u}} &= 4\mu(\hat{x}^2-\hat{y}^2)\delta(\hat{u})/\hat{\rho}^4, \\ R_{\hat{x}\hat{u}\hat{y}\hat{u}} &= 8\mu\hat{x}\hat{y}\delta(\hat{u})/\hat{\rho}^4, \\ R_{\hat{y}\hat{u}\hat{y}\hat{u}} &= 4\mu(\hat{y}^2-\hat{x}^2)\delta(\hat{u})/\hat{\rho}^4, \end{aligned} \tag{2.6}$$

together with the components found from these by the use of symmetry operations. With our conventions,

$$Z^a{}_{;dc} - Z^a{}_{;cd} = R^a{}_{bcd}Z^b \tag{2.7}$$

for any vector field Z^a, where a semicolon denotes covariant differentiation. The $\delta(\hat{u})$ behavior of the Riemann tensor implies that the shock is impulsive in the terminology of Penrose.[7]

Returning to the metric form (2.2), we see from Eq. (2.3) that the two pieces of Minkowski space on either side of the shock have been joined with a warp. For example, any geodesic crossing the shock will be a continuous curve in $(\hat{u},\hat{v},\hat{x},\hat{y})$ coordinates, so that the value of v along the curve will change discontinuously by $8\mu\ln\hat{\rho}$ at the shock, while x and y do not jump. Geodesics crossing the shock will also be deflected, when viewed in

(u, v, x, y) coordinates. Such a geodesic will have a continuous tangent vector in $(\hat{u}, \hat{v}, \hat{x}, \hat{y})$ coordinates; its deflection will be found from the differential coordinate transformation at the shock. This transformation matrix will define a Lorentz transformation, since the metric form (2.5) is Minkowskian just behind the shock. The Lorentz transformation is

$$\begin{aligned} dt &= (1+8\mu^2\hat{\rho}^{-2})d\hat{t} - 4\mu\hat{x}\,\hat{\rho}^{-2}d\hat{x} \\ &\quad -4\mu\hat{y}\hat{\rho}^{-2}d\hat{y} + 8\mu^2\hat{\rho}^{-2}d\hat{z}\,, \\ dx &= -4\mu\hat{x}\hat{\rho}^{-2}d\hat{t} + d\hat{x} - 4\mu\hat{x}\hat{\rho}^{-2}d\hat{z}\,, \\ dy &= -4\mu\hat{y}\hat{\rho}^{-2}d\hat{t} + d\hat{y} - 4\mu\hat{y}\hat{\rho}^{-2}d\hat{z}\,, \\ dz &= -8\mu^2\hat{\rho}^{-2}d\hat{t} + 4\mu\hat{x}\,\hat{\rho}^{-2}d\hat{x} \\ &\quad + 4\mu\hat{y}\hat{\rho}^{-2}d\hat{y} + (1-8\mu^2\hat{\rho}^{-2})d\hat{z}\,, \end{aligned} \tag{2.8}$$

where

$$\hat{u} = \hat{z} + \hat{t}, \quad \hat{v} = \hat{z} - \hat{t}\,. \tag{2.9}$$

We shall need this transformation in order to find the effect of shock 2 on shock 1.

Next we consider the detailed shock structure which is present when γ is large but not infinite. We now wish to describe a Schwarzschild black hole moving in the positive z direction at speed β close to 1, in the region of thickness $O(\gamma^{-1})$ close to the plane $\{z = \beta t\}$. For later convenience in studying the interaction problem, we have chosen to describe the detailed structure of a shock which moves in the opposite direction to the impulsive shock just discussed. Thus we shall make statements about asymptotic behavior of the one-parameter family of Schwarzschild spacetimes with $M = \mu/\gamma$, which are valid as t, x, y, z, and $\gamma(z-\beta t)$ tend to constants, while $\gamma \to \infty$ with μ fixed.

Starting from the isotropic form (2.1) of the Schwarzschild metric, we make a Lorentz boost

$$\bar{t} = \gamma(t' - \beta z'), \quad \bar{x} = x', \quad \bar{y} = y', \quad \bar{z} = \gamma(z' - \beta t')\,, \tag{2.10}$$

where

$$\bar{x} = \bar{r}\sin\theta\cos\phi, \quad \bar{y} = \bar{r}\sin\theta\sin\phi, \quad \bar{z} = \bar{r}\cos\theta\,, \tag{2.11}$$

to arrive at an asymptotic expansion for the metric in the shock:

$$\begin{aligned} g_{t't'} &= (4\mu/\bar{r})\gamma - (1 + \mu^2/2\bar{r}^2) \\ &\quad + (2\mu^3/\bar{r}^3 - 2\mu/\bar{r})\gamma^{-1} + O(\gamma^{-2})\,, \\ g_{t'x'} &= g_{t'y'} = 0\,, \\ g_{t'z'} &= -(4\mu/\bar{r})\gamma + (\mu^2/2\bar{r}^2) \\ &\quad + (2\mu/\bar{r} - 2\mu^3/\bar{r}^3)\gamma^{-1} + O(\gamma^{-2})\,, \\ g_{x'x'} &= 1 + (2\mu/\bar{r})\gamma^{-1} + O(\gamma^{-2})\,, \\ g_{x'y'} &= g_{x'z'} = 0\,, \\ g_{y'y'} &= 1 + (2\mu/\bar{r})\gamma^{-1} + O(\gamma^{-2})\,, \\ g_{y'z'} &= 0\,, \\ g_{z'z'} &= (4\mu/\bar{r})\gamma + (1 - \mu^2/2\bar{r}^2) \\ &\quad + (2\mu^3/\bar{r}^3 - 2\mu/\bar{r})\gamma^{-1} + O(\gamma^{-2})\,. \end{aligned} \tag{2.12}$$

This metric can be treated further so as to remove all the γ^1 and γ^0 parts except for the Minkowskian diag$(-1, 1, 1, 1)$. First we remove the γ^1 parts by using a coordinate transformation

$$\begin{aligned} t' &= t'' - 2\mu\ln[r'' + \gamma(z'' - \beta t'')] \\ &\quad + 4\mu^2\gamma^{-1}[r'' - \gamma(z'' - \beta t'')](\rho'')^{-2}\,, \\ x' &= x'' - 2\mu\gamma^{-1}[r'' - \gamma(z'' - \beta t'')]x''(\rho'')^{-2}\,, \\ y' &= y'' - 2\mu\gamma^{-1}[r'' - \gamma(z'' - \beta t'')]y''(\rho'')^{-2}\,, \\ z' &= z'' - 2\mu\beta\ln[r'' + \gamma(z'' - \beta t'')] \\ &\quad + 4\mu^2\beta\gamma^{-1}[r'' - \gamma(z'' - \beta t'')](\rho'')^{-2}\,, \end{aligned} \tag{2.13}$$

where

$$\begin{aligned} (r'')^2 &= (x'')^2 + (y'')^2 + \gamma^2(z'' - \beta t'')^2\,, \\ (\rho'')^2 &= (x'')^2 + (y'')^2\,. \end{aligned} \tag{2.14}$$

This leads to a metric

$$\begin{aligned} g_{t''t''} &= -1 + \tfrac{15}{2}\mu^2(r'')^{-2} - 8\mu^2\gamma(z'' - \beta t'')(r'')^{-3} \\ &\quad + O(\gamma^{-1})\,, \\ g_{t''x''} &= O(\gamma^{-1})\,, \\ g_{t''y''} &= O(\gamma^{-1})\,, \\ g_{t''z''} &= -\tfrac{15}{2}\mu^2(r'')^{-2} + 8\mu^2\gamma(z'' - \beta t'')(r'')^{-3} + O(\gamma^{-1})\,, \\ g_{x''x''} &= 1 + \gamma^{-1}(y''^2 - x''^2)\, f(\rho'', \gamma(z'' - \beta t'')) \\ &\quad + O(\gamma^{-2})\,, \\ g_{x''y''} &= -2\gamma^{-1}x''y''f(\rho'', \gamma(z'' - \beta t'')) + O(\gamma^{-2})\,, \\ g_{x''z''} &= O(\gamma^{-1})\,, \\ g_{y''y''} &= 1 + \gamma^{-1}(x''^2 - y''^2)\, f(\rho'', \gamma(z'' - \beta t'')) \\ &\quad + O(\gamma^{-2})\,, \\ g_{y''z''} &= O(\gamma^{-1})\,, \\ g_{z''z''} &= 1 + \tfrac{15}{2}\mu^2(r'')^{-2} - 8\mu^2\gamma(z'' - \beta t'')(r'')^{-3} + O(\gamma^{-1})\,, \end{aligned} \tag{2.15}$$

where the function f is defined by

$$f(p,q)=4\mu[q-(p^2+q^2)^{1/2}]p^{-4}$$
$$+2\mu(p^2+q^2)^{-1/2}p^{-2}. \tag{2.16}$$

Next the geometry can be put in the form of a Minkowski metric plus corrections of $O(\gamma^{-1})$, using a coordinate transformation close to the identity:

$$t''=t'''-\tfrac{15}{4}\mu^2\gamma^{-1}(\rho''')^{-1}\arctan[\gamma(z'''-\beta t''')/\rho''']$$
$$-4\mu^2\gamma^{-1}/\gamma''',$$
$$x''=x''',$$
$$y''=y''', \tag{2.17}$$
$$z''=z'''-\tfrac{15}{2}\mu^2\gamma^{-1}(\rho''')^{-1}\arctan[\gamma(z'''-\beta t''')/\rho''']$$
$$-4\mu^2\gamma^{-1}/\gamma''',$$

which removes the extra γ^0 terms in $g_{t''t''}$, $g_{t''z''}$, and $g_{z''z''}$. Here

$$(\gamma''')^2=(x''')^2+(y''')^2+\gamma^2(z'''-\beta t''')^2,$$
$$(\rho''')^2=(x''')^2+(y''')^2. \tag{2.18}$$

Finally, a coordinate transformation can be made which removes all γ^{-1} corrections to the Minkowski metric η_{ab}, except for those in the transverse components $g_{\hat{x}\hat{x}}$, $g_{\hat{x}\hat{y}}$, and $g_{\hat{y}\hat{y}}$. We arrive at the asymptotic expansion

$$g_{ab}(\hat{t},\hat{x},\hat{y},\hat{z},\gamma)=\eta_{ab}+\gamma^{-1}h^{(1)}_{ab}(\hat{x},\hat{y},\gamma(\hat{z}-\beta\hat{t}))$$
$$+\gamma^{-2}h^{(2)}_{ab}(\hat{x},\hat{y},\gamma(\hat{z}-\beta\hat{t}))+\cdots, \tag{2.19}$$

where the only nonzero components of $h^{(1)}_{ab}$ are

$$h^{(1)}_{\hat{x}\hat{x}}=(\hat{y}^2-\hat{x}^2)f(\hat{\rho},\gamma(\hat{z}-\beta\hat{t})),$$
$$h^{(1)}_{\hat{x}\hat{y}}=-2\hat{x}\hat{y}\,f(\hat{\rho},\gamma(\hat{z}-\beta\hat{t})), \tag{2.20}$$
$$h^{(1)}_{\hat{y}\hat{y}}=(\hat{x}^2-\hat{y}^2)f(\hat{\rho},\gamma(\hat{z}-\beta\hat{t})),$$

and the function f is defined in Eq. (2.16). This is the most useful form for the detailed shock structure in the region where $\hat{t}$, $\hat{\rho}$, $\hat{z}$, and $\gamma(\hat{z}-\beta\hat{t})$ are of $O(1)$.

We remark that $h^{(1)}_{ab}$ tends to zero as we move well ahead of the shock, with $\gamma(\hat{z}-\beta\hat{t})\to+\infty$. But as we let $\gamma(\hat{z}-\beta\hat{t})\to-\infty$, moving well behind the shock, $h^{(1)}_{ab}$ grows linearly with $\gamma(\hat{z}-\beta\hat{t})$. This behavior has been designed for matching onto the impulsive shock geometry in the C^0 form (2.5), which should give an accurate description of the metric once we let $|\gamma(\hat{z}-\beta\hat{t})|$ become so large that $|\hat{z}-\hat{t}|$ is of $O(1)$. For this purpose we must replace $\hat{u}$ by $-\hat{v}$ and $\hat{v}$ by $-\hat{u}$ in Eq. (2.5), while keeping $\hat{u}=\hat{z}+\hat{t}$, $\hat{v}=\hat{z}-\hat{t}$, so that the impulsive $\gamma=\infty$ shock also moves in the positive $\hat{z}$ direction. Then the linear behavior of the combination

$$\gamma^{-1}(h^{(1)}_{\hat{x}\hat{x}}+ih^{(1)}_{\hat{x}\hat{y}})\sim 8\mu\gamma^{-1}(\hat{y}-i\hat{x})^2\gamma(\hat{z}-\beta\hat{t})$$
$$\times\theta(\gamma(\beta\hat{t}-\hat{z}))(\hat{\rho})^{-4}$$

when $|\gamma(\hat{z}-\beta\hat{t})|$ is large matches precisely onto the $\hat{v}\theta(-\hat{v})$ terms near the shock in the impulsive metric (2.5). One might wish to extend this desirable property so that $g_{ab}(\hat{t},\hat{x},\hat{y},\hat{z},\gamma)$ in the shock region matches out to the complete impulsive $\gamma=\infty$ metric (2.5) with $O(\gamma^{-1})$ corrections, in the region where $\hat{t}$, $\hat{\rho}$, $\hat{z}$, and $(\hat{z}-\hat{t})$ are of $O(1)$. This could presumably be done by using some of the coordinate freedom in choosing $h^{(2)}_{ab}$ to arrange for the correct $\gamma^{-2}[\gamma(\hat{z}-\beta\hat{t})]^2\theta(\gamma(\beta\hat{t}-\hat{z}))$ behavior in $\gamma^{-2}h^{(2)}_{ab}$, and by choosing $h^{(n)}_{ab}$ for $n>2$ to increase less rapidly than $[\gamma(\hat{z}-\beta\hat{t})]^n$ as $|\gamma(\hat{z}-\beta\hat{t})|\to\infty$.

The leading curvature terms in the shock region were found originally by Pirani.[8] These are $O(\gamma)$, and reside in the components $R_{\hat{x}\hat{v}\hat{x}\hat{v}}$, $R_{\hat{x}\hat{v}\hat{y}\hat{v}}$, and $R_{\hat{y}\hat{v}\hat{y}\hat{v}}$, together with the components found from these by symmetry operations. We have

$$R_{\hat{x}\hat{v}\hat{x}\hat{v}}=3\gamma\mu(\hat{y}^2-\hat{x}^2)[\hat{x}^2+\hat{y}^2+\gamma^2(\hat{z}-\beta\hat{t})^2]^{-5/2}$$
$$+O(1),$$
$$R_{\hat{x}\hat{v}\hat{y}\hat{v}}=-6\gamma\mu\hat{x}\hat{y}[\hat{x}^2+\hat{y}^2+\gamma^2(\hat{z}-\beta\hat{t})^2]^{-5/2} \tag{2.21}$$
$$+O(1),$$
$$R_{\hat{y}\hat{v}\hat{y}\hat{v}}=3\gamma\mu(\hat{x}^2-\hat{y}^2)[\hat{x}^2+\hat{y}^2+\gamma^2(\hat{z}-\beta\hat{t})^2]^{-5/2}$$
$$+O(1)$$

in the shock region, found from the second derivatives $h^{(1)}_{ab,\hat{v}\hat{v}}$. These leading $O(\gamma)$ curvature terms are of Petrov type N, when taken by themselves, and their net effect on integration through the $O(\gamma^{-1})$ shock thickness is to produce the δ-function impulsive shock strength given in Eq. (2.6), after allowing for the reversed direction of motion. But note that the curvature (2.21) in the smeared-out shock at finite γ still has the $(\hat{r})^{-3}$ behavior at large spatial distances, characteristic of asymptotically flat spacetimes. It is only when we take the limit $\gamma\to\infty$ that we reach a plane-fronted metric with $(\hat{r})^{-2}$ falloff in the curvature, due to the loss of a spatial dimension.

III. EVOLUTION OF THE CURVED SHOCKS BY GEOMETRICAL OPTICS

We now turn to the interaction problem in which black hole 1 moves initially in the positive z direction, and black hole 2 moves in the negative z direction, both with energy μ at large γ_1,γ_2. At present, we allow the impact parameter to scale as $O(1)$ when $\gamma_1,\gamma_2\to\infty$; in other words, the impact parameter is to be of the general size μ. We start by describing the geometry of the shocks in the speed-of-light collision, and then consider the evolution of the detailed shock structure after a collision at finite γ_1,γ_2 in the special axisymmetric case with zero impact parameter.

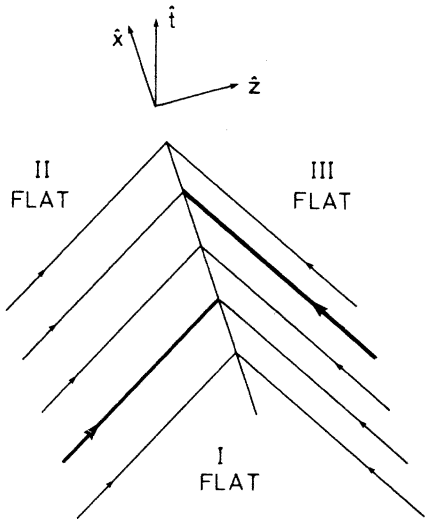

FIG. 2. The two null shocks are shown approaching before the collision; one spatial dimension has been suppressed. The incoming shock 1 lies on the surface $\{\hat{z}=\hat{t}\}$ separating the flat regions I and II, while shock 2 lies on the surface $\{\hat{z}=-\hat{t}\}$ between the flat regions I and III. Some null generators have been drawn on each null surface; the heavy lines show the null world lines at the center of the shocks—these are all that remain of the black holes after boosting to the speed of light. In the collision drawn here, the central world lines do not intersect, and the spacetime is nonaxisymmetric.

The situation before the collision of the impulsive shocks at $\gamma=\infty$ is depicted in Fig. 2. Using the C^0 form (2.5) of the metric for a single impulsive shock, we can write the precollision metric as

$$\begin{aligned} ds^2 &= d\hat{u}\,d\hat{v}+[1-4\mu\hat{u}\theta(\hat{u})(\hat{\rho})^{-2}]^2 d\hat{\rho}^2 \\ &\quad +[8\mu\hat{v}\theta(-\hat{v})(\hat{\rho}_1)^{-2}+16\mu^2(\hat{v})^2\theta(-\hat{v})(\hat{\rho}_1)^{-4}]\,d\hat{\rho}_1^{\,2} \\ &\quad +\hat{\rho}^2[1+4\mu\hat{u}\theta(\hat{u})(\hat{\rho})^{-2}]^2 d\phi^2 \\ &\quad +\hat{\rho}_1^{\,2}[-8\mu\hat{v}\theta(-\hat{v})(\hat{\rho}_1)^{-2} \\ &\qquad +16\mu^2(\hat{v})^2\theta(-\hat{v})(\hat{\rho}_1)^{-4}]\,d\phi_1^{\,2}\ , \end{aligned} \tag{3.1}$$

where

$$\begin{aligned} &\hat{u}=\hat{z}+\hat{t},\quad \hat{v}=\hat{z}-\hat{t}\ , \\ &\hat{\rho}_1\cos\phi_1=\hat{\rho}\cos\phi+a,\quad \hat{\rho}_1\sin\phi_1=\hat{\rho}\sin\phi\ . \end{aligned} \tag{3.2}$$

This form of the metric will be valid in region I ($\hat{u}<0$, $\hat{v}>0$) between the two incoming shocks, in a neighborhood of shock 1 extending into region II ($\hat{u}<0,\hat{v}<0$), and in a neighborhood of shock 2 extending into region III ($\hat{u}>0,\hat{v}>0$). When $\hat{v}>0$, it reduces to Eq. (2.5), and when $\hat{u}<0$ it reduces to the metric (2.5) with the shock moving in the opposite direction, so that $\hat{u}\to-\hat{v}$, $\hat{v}\to-\hat{u}$. Here a is the impact parameter.

To find the continuation of (say) shock 1 after its collision with shock 2, we follow the null geodesic generators through the spacelike collision two-surface $\{\hat{u}=\hat{v}=0\}$. As explained in Sec. II, a geodesic passing through shock 2 can be described in (u,v,x,y) coordinates as suffering a jump of $8\mu\ln\rho$ and a deflection produced by the Lorentz transformation (2.8) at the shock, while the geodesic is a C^1 curve when viewed in $(\hat{u},\hat{v},\hat{x},\hat{y})$ coordinates. Since the incoming generators of shock 1 have $d\hat{z}/d\hat{t}=1$, $d\hat{x}/d\hat{t}=0$, $d\hat{y}/d\hat{t}=0$, the curved shock 1 can be given the parametric representation

$$\begin{aligned} t&=-2\mu\ln(\xi^2+\eta^2)+[1+16\mu^2/(\xi^2+\eta^2)]\lambda\ , \\ x&=\xi-8\mu\xi\lambda/(\xi^2+\eta^2)\ , \\ y&=\eta-8\mu\eta\lambda/(\xi^2+\eta^2)\ , \\ z&=2\mu\ln(\xi^2+\eta^2)+[1-16\mu^2/(\xi^2+\eta^2)]\lambda\ . \end{aligned} \tag{3.3}$$

Here $\lambda\geq 0$ is an affine parameter along each of the null geodesic generators, and (ξ,η) give the values of (x,y) on the geodesic at the collision. Curved

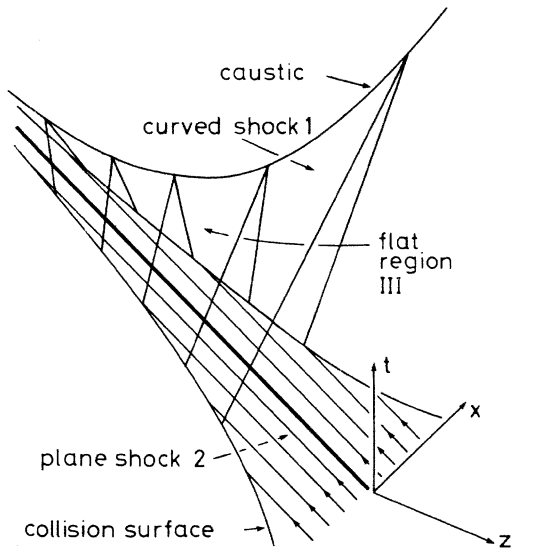

FIG. 3. In an axisymmetric collision at the speed of light, the region III of flat spacetime is bounded by the plane shock 2 and the curved shock 1. One spatial dimension has been suppressed, and the coordinates are Minkowskian for region III. Some null generators of shock 2 have been drawn, including the heavy line at the center of the shock. Each null generator of shock 2 eventually meets shock 1 on the collision surface, which is two-dimensional, spacelike, and noncompact. In the diagram, the collision surface appears as a pair of lines. The null generators of the curved shock 1 emerge through the collision surface, and come to a focus on the caustic region at the top of the diagram. The caustic region is a spacelike line which becomes asymptotically null at both ends, and lies on the axis of symmetry.

shock 2 can be described in a similar way. The geometry of the curved shocks was first found by Penrose.

Figure 3 shows how region III is bounded by part of the plane $\{z+t=0\}$ and by the achronal curved shock 1. This achronal set contains a one-dimensional spacelike caustic region on the axis $\rho=(x^2+y^2)^{1/2}=0$, given by

$$z-t=4\mu\ln[4\mu(z+t)]-4\mu\ , \tag{3.4}$$

where the generators of curved shock 1 have been focused by shock 2 and intersect each other. At large values of ρ the geodesics have been deflected toward the axis by a small angle of approximately $8\mu/\rho$. Correspondingly, the curved shock surface has the logarithmic shape

$$z=t+8\mu\ln\rho+o(1) \tag{3.5}$$

as $\rho\to\infty$ with t fixed. As we consider geodesics which start with smaller and smaller ρ values, the deflection becomes larger; for a geodesic starting at $\rho=4\mu$, dz/dt is zero, and for smaller ρ values dz/dt is negative. The caustic region becomes asymptotically null, with $dz/dt\to+1$, in the region where geodesics starting from large ρ values hit the axis. But the other end of the caustic region, due to geodesics from small ρ values hitting the axis, is asymptotic to the surface $\{z+t=0\}$. One expects that a spacetime singularity will be produced by the infinite focusing at the caustic region in the speed-of-light collision. This would lead to a loss of predictability of the geometry to the future of the caustic region; for example, there may be a Cauchy horizon on the null surface formed by continuing the generators of curved shock 1 through the caustic region. However, when the collision is at finite γ_1,γ_2, we shall see that the metric can remain quite smooth near the caustic region and beyond.

An alternative view of curved shock 1 is provided in Figs. 4(a), 4(b), and 4(c) which give three successive snapshots of the shock at different

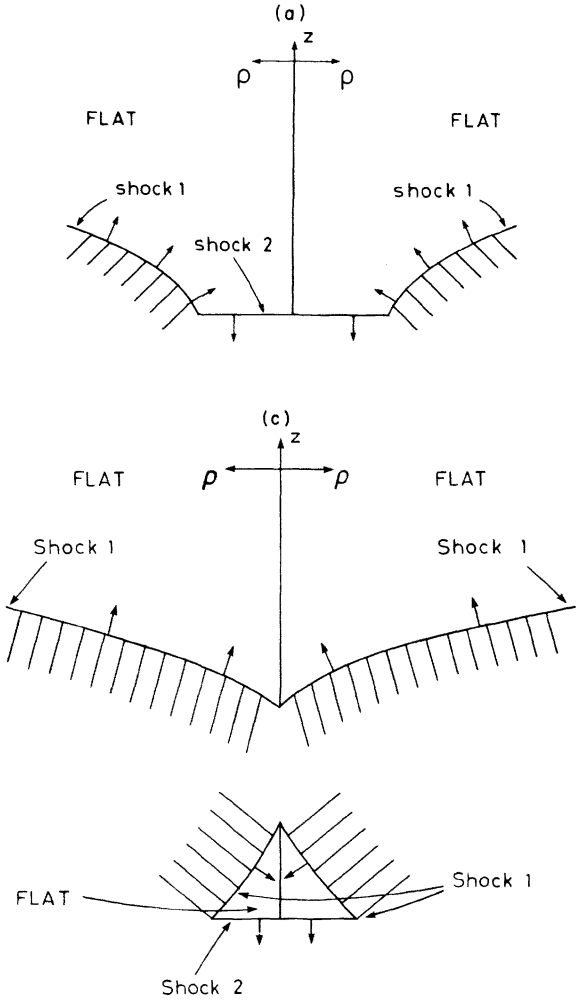

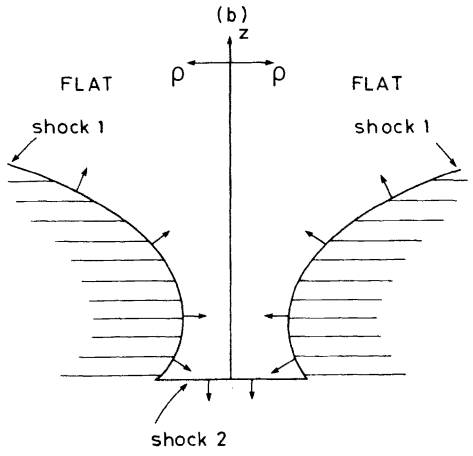

FIG. 4. (a), (b), and (c) The curved shock 1 is seen at three successive times t as it moves at the speed of light into the flat region III. The diagrams show the instantaneous shock front in a neighborhood of the symmetry axis; z measures distance along the axis, and ρ measures distance away from the axis in the Minkowskian region III. Also shown is the plane front of shock 2, which moves down the axis at the speed of light. The arrows on the shocks give their direction of motion. At the earliest time (a) all of shock 1 moves in the positive z direction; the null generators which have been deflected by the largest angle are those which were closest to the axis at the collision with shock 2—further out from the axis the shock front has a logarithmic shape. Later (b) shock 2 has moved down to reveal a part of shock 1 which moves in the negative z direction, due to the very strong deflection produced near the axis. Still later (c), shock 1 has reached the axis; one part of shock 1 moves upward, and the other downward. Shock 1 meets the axis at the caustic region, which travels along the axis at more than the speed of light.

times t.

Next we wish to describe the detailed behavior of the curved shocks produced by an axisymmetric collision at speeds less than 1. A similar but more complicated description could also be given for the shock dynamics when the impact parameter $a \neq 0$. For simplicity we shall further assume, in this and in the following sections, that the two incoming black holes have equal masses M and hence the same factor $\gamma = \mu/M$. The extension to the case of unequal but comparable masses M_1, M_2, given by the scaling $\gamma_1 = \gamma c_1$, $\gamma_2 = \gamma c_2$ along a family with $\gamma \to \infty$, is always straightforward and will be mentioned whenever appropriate.

At early times before the collision, the detailed structure of shock 1 will be described by the expansion (2.19) and (2.20), together with corrections tending to zero rapidly as $\hat{t} \to -\infty$, due to the field of black hole 2, which can be felt slightly by black hole 1 before the collision when γ is finite. Similarly, the detailed structure of shock 2 will be represented by Eqs. (2.19) and (2.20), with β replaced by $-\beta$, apart from terms giving early warning of the arrival of black hole 1. At finite γ, the collision no longer takes place on a spacelike two-surface. Instead, the collision will be smeared out over a region at separations of $O(\gamma^{-1})$ away from the surface $\{\hat{z} = \hat{t} = 0\}$. This leads us to set up an asymptotic expansion in $(\hat{t}, \hat{x}, \hat{y}, \hat{z})$ coordinates:

$$g_{ab}(\hat{t},\hat{x},\hat{y},\hat{z},\gamma) = \eta_{ab} + \gamma^{-1} k_{ab}^{(1)}(\gamma\hat{t},\hat{x},\hat{y},\gamma\hat{z}) + \gamma^{-2} k_{ab}^{(2)}(\gamma\hat{t},\hat{x},\hat{y},\gamma\hat{z}) + \cdots , \tag{3.6}$$

which is valid as $\gamma\hat{t}, \hat{x}, \hat{y}, \gamma\hat{z} \to$ constants, with $\gamma \to \infty$. The vacuum field equations in this region are of the form

$$\mathcal{L}[k_{ab}^{(n)}] = \mathcal{F}^{(n)}[k_{ab}^{(1)}, \ldots, k_{ab}^{(n-1)}] , \tag{3.7}$$

where $\mathcal{L}$ is a linear operator involving only second derivatives with respect to the variables $(\gamma\hat{t})$ and $(\gamma\hat{z})$, while $\mathcal{F}^{(n)}$ is a functional of the lower-order perturbations $k_{ab}^{(1)}, \ldots, k_{ab}^{(n-1)}$, involving their derivatives. In particular, $k_{ab}^{(1)}$ satisfies a linear homogeneous field equation. The boundary conditions on this expansion are that it should reduce to Eqs. (2.19) and (2.20) for the incoming shock 1, when we let $(\gamma\hat{t}) \to -\infty$ and $(\gamma\hat{z}) \to -\infty$ in such a way that $\gamma(\hat{z} - \beta\hat{t})$ remains finite, and a corresponding condition for matching onto the expansion for the detailed structure of the incoming shock 2.

Because of the linearity of the lowest-order field equation, we see that

$$k_{ab}^{(1)}(\gamma\hat{t},\hat{x},\hat{y},\gamma\hat{z}) = h_{ab}^{(1)}(\hat{x},\hat{y},\gamma(\hat{z}-\hat{t})) + h_{ab}^{(1)}(\hat{x},\hat{y},\gamma(\hat{z}+\hat{t})) , \tag{3.8}$$

apart from possible gauge terms, where the function $h_{ab}^{(1)}$ is defined by Eqs. (2.20), (2.16). The removal of the coefficient β in the arguments of $h_{ab}^{(1)}$ is permissible since $\beta = 1 - \frac{1}{2}\gamma^{-2} + O(\gamma^{-4})$. The linearity of Eq. (3.8) is deceptive; it does not mean that the shocks have failed to interact. In fact shock 1 (say) emerges through shock 2 into a region where the coordinates $(\hat{t}, \hat{x}, \hat{y}, \hat{z})$ are not Minkowskian. To understand the interaction of the shocks more clearly, we should transform to coordinates (t, x, y, z) which show that the region behind shock 2 is almost flat before the arrival of curved shock 1. Thus we should follow shock 1 through the collision to points where $\hat{x}, \hat{y}, \gamma(\hat{z} - \hat{t})$ are of $O(1)$ but $\gamma(\hat{z} + \hat{t}) \gg 1$, so that we are well past the detailed structure of shock 2, and into the region where shock 2 can be accurately represented by Eq. (2.5). If we then make the transformation (2.3), so that the metric due to shock 2 becomes manifestly flat, then the leading corrections to flat space will be found by transforming $\gamma^{-1} h_{ab}^{(1)}(\hat{x}, \hat{y}, \gamma(\hat{z} - \hat{t}))$. Using the inverse of the Lorentz transformation (2.8), we find that $h_{ab}^{(1)}(\hat{x}, \hat{y}, \gamma(\hat{z} - \hat{t}))$ is given in (t, x, y, z) coordinates just behind the shock 2 by

$$\begin{aligned} &h_{tt}^{(1)} = -16\mu^2 f, \quad h_{tx}^{(1)} = -4\mu\xi f , \\ &h_{ty}^{(1)} = -4\mu\eta f, \quad h_{tz}^{(1)} = -16\mu^2 f , \\ &h_{xx}^{(1)} = (\eta^2 - \xi^2) f, \quad h_{xy}^{(1)} = -2\xi\eta f, \quad h_{xz}^{(1)} = -4\mu\xi f , \\ &h_{yy}^{(1)} = (\xi^2 - \eta^2) f , \quad h_{yz}^{(1)} = -4\mu\eta f, \quad h_{zz}^{(1)} = -16\mu^2 f . \end{aligned} \tag{3.9}$$

Here we follow the notation of Eq. (3.3) and write (ξ, η) for the values of (x, y) on curved shock 1 just after the collision; thus the thin curved shock is centered around $t = -2\mu \ln(\xi^2 + \eta^2)$, $z = 2\mu \ln(\xi^2 + \eta^2)$ due to the discontinuous jump produced by shock 2. Also f in Eq. (3.9) refers to $f((\xi^2 + \eta^2)^{1/2}, \gamma(\hat{z} - \hat{t}))$, with the functional form of f defined by Eq. (2.16).

The initial data for curved shock 1 just behind shock 2 can be rewritten in a more satisfactory form without mention of the variables $\hat{z}$ and $\hat{t}$. Let us represent the curved shock surface (3.3) locally by the equation $z = j(t, \rho)$. Thus we are at present working near the start of curved shock 1, where

$$j(-2\mu \ln(\xi^2 + \eta^2), (\xi^2 + \eta^2)^{1/2}) = 2\mu \ln(\xi^2 + \eta^2) . \tag{3.10}$$

Using the inverse of the Lorentz transformation (2.8), we find that in the small region occupied by curved shock 1, $\gamma(\hat{z} - \hat{t})$ can effectively be replaced by $[1 - 16\mu^2/(\xi^2 + \eta^2)]\,\gamma(z - j(t, \rho))$ just behind shock 2. Hence, in the initial data (3.9), we can

regard f as

$$f((\xi^2+\eta^2)^{1/2},[1-16\mu^2/(\xi^2+\eta^2)]\gamma(z-j(t,\rho)))\ .$$

We have now set up the initial data for the curved shock 1, showing how the detailed structure of shock 1 has been rearranged near the surface $\{z=j(t,\rho)\}$ during the collision with shock 2.

One expects that curved shock 1 will be concentrated at distances of $O(\gamma^{-1})$ away from the surface $\{z=j(t,\rho)\}$ during its evolution, just as the incoming shock was spread over a thickness of $O(\gamma^{-1})$ near the plane $\{z=t\}$. This leads one to the asymptotic expansion

$$g_{ab}(t,x,y,z,\gamma)=\eta_{ab}+\gamma^{-1}l^{(1)}_{ab}(t,x,y,\gamma(z-j(t,\rho)))+\gamma^{-2}l^{(2)}_{ab}(t,x,y,\gamma(z-j(t,\rho)))+\cdots \tag{3.11}$$

for the detailed structure of curved shock 1. The expansion should be valid as t,x,y and $\gamma(z-j(t,\rho))$ tend to constants, while $\gamma\to\infty$. The initial data just described provide a possible choice for $l^{(1)}_{ab}$ on the initial surface, unique up to the addition of gauge terms.

In order to calculate the evolution of the detailed structure for curved shock 1, we make use of the symmetries of the spacetimes. Apart from the rotational Killing vector field $\partial/\partial\phi$, the spacetimes also possess a discrete isometry $\phi\to-\phi$, inherited from the corresponding property of the incoming Schwarzschild solutions. Under these symmetry conditions we can write the components $l^{(1)}_{ab}$, giving the dominant shock structure, as

$$l^{(1)}_{tt}=A,\quad l^{(1)}_{tx}=xB,\quad l^{(1)}_{ty}=yB,\quad l^{(1)}_{tz}=C\ ,$$

$$l^{(1)}_{xx}=D+(y^2-x^2)E,\quad l^{(1)}_{xy}=-2xyE,\quad l^{(1)}_{xz}=xF\ ,$$

$$l^{(1)}_{yy}=D+(x^2-y^2)E,\quad l^{(1)}_{yz}=yF,\quad l^{(1)}_{zz}=G\ , \tag{3.12}$$

where A,B,C,D,E,F,G are functions

$$A=A(t,\rho,\gamma(z-j(t,\rho)))\ ,$$

etc. The metric can be further simplified by choice of a convenient gauge. Gauge transformations respecting the symmetrices of the spacetime involve three free functions, and we can use these to remove three of the seven functions $A,\ldots,G$ in Eqs. (3.12). We choose

$$B=D=F=0\ . \tag{3.13}$$

In describing the field equations, we write $j_t=\partial j/\partial t$, $j_\rho=\partial j/\partial\rho$. Since $\{z=j(t,\rho)\}$ is a null surface,

$$(j_t)^2=1+(j_\rho)^2\ . \tag{3.14}$$

We also label the variables $t,\rho,\gamma(z-j(t,\rho))$ as x^1,x^2,x^3, respectively. Then three of the field equations give

$$A_{33}=\rho^2E_{33},\quad C_{33}=0,\quad A_{33}+G_{33}=0\ . \tag{3.15}$$

If we require that the field $l^{(1)}_{ab}$ tends to zero well ahead of curved shock 1, when $\gamma(z-j(t,\rho))\to\infty$, then we can integrate these equations to find

$$A=\rho^2E,\quad C=0,\quad A+G=0\ . \tag{3.16}$$

Now $l^{(1)}_{ab}$ is described simply in terms of the single function E. There is one remaining field equation for E, found by combining the $R_{xx}=0$ and $R_{xy}=0$ equations. This evolution equation for the curved shock gives

$$2j_\rho E_2-2j_tE_1+(5\rho^{-1}j_\rho+j_{\rho\rho}-j_{tt})E=0\ . \tag{3.17}$$

Using the parametric equation (3.3) for the surface $\{z=j(t,\rho)\}$, we can write (3.17) as a first-order ordinary differential equation along the null generators:

$$\frac{dE}{d\lambda}=[20\mu/(\xi^2+\eta^2-8\mu\lambda)-4\mu/(\xi^2+\eta^2+8\mu\lambda)]E\ . \tag{3.18}$$

This has the general solution

$$E=K(\rho,\gamma(z-j(t,\rho)))[1-8\mu\lambda/(\xi^2+\eta^2)]^{-5/2}\times[1+8\mu\lambda/(\xi^2+\eta^2)]^{-1/2} \tag{3.19}$$

for an arbitrary function K. We see that the curved shock evolution is dominated by "geometrical optics" behavior at ρ values of $O(1)$, where each part of the shock evolves separately along its own null generator, and transverse derivatives across the generators have little effect.

A gauge transformation can be found which puts our initial data (3.9) for the detailed structure of curved shock 1 into the form (3.12) with Eqs. (3.13) and (3.16) holding. This leads to the initial condition

$$E|_{\lambda=0}=K(\rho,\gamma(z-j(t,\rho)))=f((\xi^2+\eta^2)^{1/2},[1-16\mu^2/(\xi^2+\eta^2)]\times\gamma(z-j(t,\rho))) \tag{3.20}$$

with f defined by Eq. (2.16). Together Eqs. (3.19) and (3.20) describe the evolution of $l^{(1)}_{ab}$, giving the dominant structure of curved shock 1, beyond the collision region.

Note that ρ^2E tends to infinity as $\lambda\to(\xi^2+\eta^2)/8\mu$, where shock 1 reaches the caustic region. This behavior does not necessarily imply that a spacetime singularity is reached, although it does indicate that the present asymptotic expansion (3.11) has broken down and must be matched onto another expansion which allows for some qualitatively different behavior in the caustic region, as described in the following section.

The information presented here can be used to provide characteristic initial data for the geometry in the interaction region IV. This geometry will also be described by an asymptotic expansion as $\gamma \to \infty$, where the leading term is just the metric produced by the collision at exactly the speed of light. The interaction region for the $\gamma = \infty$ problem is bounded by curved shocks 1 and 2, which are again impulsive, with δ functions in the curvature which can be found from the detailed structure just discussed by integrating across the shock.

Only a small modification is needed for the case of unequal masses. The detailed structure of curved shock 1 (say) will be represented by an expansion like Eq. (3.11), except that γ should be replaced by γ_1, so that the leading perturbation of flat space is

$$(\gamma_1)^{-1} l_{ab}^{(1)}(t, x, y, \gamma_1(z - j(t, \rho))) .$$

The functional form of $l_{ab}^{(1)}$ is unchanged.

IV. THE CAUSTIC REGION

In this section we shall consider the behavior of the gravitational field produced by the axisymmetric collision close to the spacelike caustic region $\{\rho = 0, z = j(t, 0)\}$ on the axis. We showed in Sec. III that the leading metric perturbations $\gamma^{-1} l_{ab}^{(1)}$ in curved shock 1 grow like $\gamma^{-1}\rho^2 E$ as $\rho \to 0$, where $\rho^2 E$ is proportional to $\rho^2[1 - 8\mu\lambda/(\xi^2 + \eta^2)]^{-5/2}$, which grows like $\rho^{-1/2}$ as the caustic region is approached. This singular behavior implies that the asymptotic expansion (3.11) is breaking down, and suggests that the gravitational field possesses some qualitatively different features in the caustic region. To find a qualitative change, note that in the curved shock expansion we neglected ρ derivatives along the shock by comparison with derivatives across the shock, by using the variables ρ and $\gamma(z - j(t, \rho))$. But as we approach the caustic region, ρ derivatives should gain in importance until they may be able to balance derivatives across surfaces of constant $[z - j(t, \rho)]$. To investigate this possibility, we examine the detailed structure of the region at distances of $O(\gamma^{-1})$ away from the line $\{\rho = 0, z = j(t, 0)\}$, allowing for rapid variations in two independent directions. We shall see how the shock can interact strongly with itself in this region so as to avoid forming a singularity.

The asymptotic expansion for the caustic region should be valid as $t, \gamma\rho, \gamma(z - j(t, 0)) \to$ constants, while $\gamma \to \infty$. If this expansion is to match onto Eq. (3.11) for curved shock 1, when $(\gamma\rho) \to \infty$, we shall need half-integral powers of γ to allow for the $\gamma^{-1}\rho^{-1/2} = \gamma^{-1/2}(\gamma\rho)^{-1/2}$ growth of $\gamma^{-1} l_{ab}^{(1)}$ as $\rho \to 0$ in the intermediate matching region where $\rho \ll 1$ but $\gamma\rho \gg 1$. Thus we consider the expansion

$$g_{ab}(t, x, y, z, \gamma) = \eta_{ab} + \gamma^{-1/2} m_{ab}^{(1)}(t, \gamma\rho, \gamma(z - j(t, 0))) + \gamma^{-1} m_{ab}^{(2)}(t, \gamma\rho, \gamma(z - j(t, 0))) + \gamma^{-3/2} m_{ab}^{(3)}(t, \gamma\rho, \gamma(z - j(t, 0))) + \cdots . \quad (4.1)$$

Fixing attention on the leading perturbations $\gamma^{-1/2} m_{ab}^{(1)}$, we can exploit the symmetries of the spacetime and make gauge transformations so that $m_{ab}^{(1)}$ is described by four functions A, C, E, G of $t, \gamma\rho$ and $\gamma(z - j(t, 0))$:

$$m_{tt}^{(1)} = A, \quad m_{tx}^{(1)} = m_{ty}^{(1)} = 0, \quad m_{tz}^{(1)} = C ,$$
$$m_{xx}^{(1)} = \gamma^2(y^2 - x^2)E, \quad m_{xy}^{(1)} = -2\gamma^2 xyE, \quad m_{xz}^{(1)} = 0 ,$$
$$m_{yy}^{(1)} = \gamma^2(x^2 - y^2)E, \quad m_{yz}^{(1)} = 0, \quad m_{zz}^{(1)} = G . \quad (4.2)$$

Because of the rapid variations in two independent directions implied by the presence of the arguments $\gamma\rho$ and $\gamma(z - j(t, 0))$, the gravitational field resembles locally a cylindrical Einstein-Rosen wave.[9] The spacelike nature of the caustic region implies that $[j_t(t, 0)]^2 > 1$ and hence that the field equations in the caustic region are actually wavelike rather than elliptic. Note also that the curvature has reached a size of $\gamma^{-1/2}(\gamma)^2 = O(\gamma^{3/2})$ owing to second derivatives of $\gamma^{-1/2} m_{ab}^{(1)}$. This shows that the gravitational field is stronger here than in any other region which we have considered, owing to the focusing effect: The curvature components are only of $O(\gamma)$ in the plane and curved shocks, and only of $O(1)$ in the interaction zone just behind the curved shocks.

Boundary conditions on the field in the caustic region are provided by matching out in timelike and null directions to the past of the caustic region. This leads us into the nearly flat region ahead of curved shock 1 and into the detailed structure of curved shock 1. In particular, the field is quite smooth on the axis in the matching region. Hence we should impose a condition of regularity at the axis $\{\gamma\rho = 0\}$ on the solution $m_{ab}^{(1)}$ of the linear field equations for A, C, E, G.

In describing the field equations for the caustic region, let us write

$$X^1 = t, \quad X^2 = \gamma\rho, \quad X^3 = \gamma(z - j(t,0)) \ . \tag{4.3}$$

Then two of the field equations for $m^{(1)}_{ab}$ give

$$\begin{aligned} &C_{22} + C_2/X^2 = 0 \ , \\ &(A_{22} + G_{22}) + (A_2 + G_2)/X^2 = 0 \ . \end{aligned} \tag{4.4}$$

Since A, C, and G must be regular on the axis, the solutions are of the form

$$C = L(X^1, X^3), \quad (A + G) = N(X^1, X^3) \tag{4.5}$$

for some functions L, N. But now we can use a gauge transformation by a vector field $\gamma^{-3/2}\,\xi^a$, such that only $\xi^t = \xi^t(X^1, X^3)$ and $\xi^z = \xi^z(X^1, X^3)$ are nonzero, in order to ensure

$$C = 0, \quad (A + G) = 0 \ , \tag{4.6}$$

while preserving the form (4.2).

The remaining equations give

$$A_{22} - (j_\rho)^2 A_{33} + A_2/X^2 = 0 \ , \tag{4.7a}$$

$$A_{23} - (X^2)^2 E_{23} - 4X^2 E_3 = 0 \ , \tag{4.7b}$$

$$A_{22} - A_2/X^2 - (X^2)^2 (j_\rho)^2 E_{33} = 0 \ , \tag{4.7c}$$

$$2A_2/X^2 - (X^2)^2 E_{22} - (X^2)^2 (j_\rho)^2 E_{33} - 7X^2 E_2 - 8E = 0 \ , \tag{4.7d}$$

where $j_\rho = j_\rho(t,0)$. These equations can be shown to be all compatible. As for exact Einstein-Rosen waves, one first solves a cylindrical wave equation (4.7a), and then finds the other metric functions by quadrature.

We solve Eq. (4.7a) by use of a Green's function. First make the change of variables

$$p = j_\rho X^2 - X^3, \quad q = j_\rho X^2 + X^3 \ , \tag{4.8}$$

to put Eq. (4.7a) in the standard Euler-Darboux form

$$2(p+q)A_{pq} + A_p + A_q = 0 \ . \tag{4.9}$$

To be specific, consider the part of the caustic region which moves up the z axis [see Fig. 4(c)]. Then $j_\rho > 0$, and the domain of Eq. (4.9) is

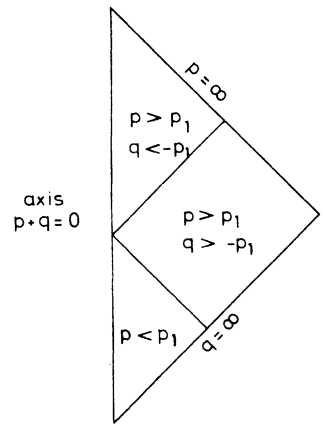

FIG. 5. The domain of the coordinates p, q, used in describing the caustic region. The domain is bounded by the axis $\{p+q=0\}$ and the two "null infinities" $\{q=\infty\}$, $\{p=\infty\}$; waves are fed into the caustic region at $q=\infty$ by shock 1, and then interact with themselves before emerging in another shock behind the caustic region, at $p=\infty$. Also shown are the three domains appearing in Eq. (4.19).

$\{p+q \geq 0\}$. The Green's function must be adapted to the boundary conditions on A, found via matching. Apart from regularity of A on the axis $\{p+q=0\}$, we require that $A \to 0$ rapidly in "time-like" directions with $p \to -\infty$, $q \to +\infty$ (see Fig. 5), for this corresponds to matching out into the nearly flat region of spacetime ahead of the caustic region and of curved shock 1. The input for the cylindrical wave equation is found by matching out in "null" directions with $p \to$ const, $q \to +\infty$, since this takes us essentially along the generators of curved shock 1, which is feeding waves into the caustic region. By matching in from curved shock 1, we find

$$A(p,q) \sim q^{-1/2} h(p) \tag{4.10}$$

as $p \to$ const, $q \to \infty$, where

$$\begin{aligned} h(p) = {} & 2^{5/2}\mu^{3/2}[1 - 16\mu^2/(\xi^2+\eta^2)]^{-1/2} \\ & \times (\{\xi^2+\eta^2+[1-16\mu^2/(\xi^2+\eta^2)]^2 p^2\}^{-1/2} - 2\{\xi^2+\eta^2+[1-16\mu^2/(\xi^2+\eta^2)]^2 p^2\}^{1/2}/(\xi^2+\eta^2) \\ & - 2[1-16\mu^2/(\xi^2+\eta^2)]p/(\xi^2+\eta^2)) \ . \end{aligned} \tag{4.11}$$

Here we have used the expressions (3.19) and (3.20) for the function E in curved shock 1, and let $\lambda \to (\xi^2+\eta^2)/8\mu$ so that $\rho \to 0$.

Accordingly we look for a Green's function $H(p,q;p_1)$ satisfying (in a distributional sense)

$$2(p+q)H_{pq} + H_p + H_q = 0 \ , \tag{4.12}$$

which is regular on the axis and has the asymptotic behavior

$$H(p,q;p_1) \sim q^{-1/2}\theta(p-p_1) + o(q^{-1/2}) \tag{4.13}$$

as $q \to \infty$ with p, p_1 fixed. This will allow us to build up a solution in the form

$$A(p,q) = \int_{-\infty}^{\infty} dp_1 H(p,q;p_1) h'(p_1) . \tag{4.14}$$

Such a Green's function can be found by starting from well-known properties of the Euler-Darboux equation,[10] as used for example by Szekeres[11] in studying spacetimes which contain colliding plane gravitational waves. The Riemann-Green function used by Szekeres is adapted to a characteristic initial-value problem with data given on a pair of intersecting lines $\{p = \text{const}\}$, $\{q = \text{const}\}$, and must then be modified to cope with our problem in which initial data are given only by the incoming field at $q = \infty$.

One begins with the function

$$J(p,q;p_1) = -(p+q)^{-1/2} P_{-1/2}(1 + 2(p_1 - p)/(p+q)) \times \theta(p_1 - p) , \tag{4.15}$$

where $P_{-1/2}$ is the Legendre function of degree $-\frac{1}{2}$. This satisfies the homogeneous equation distributionally and has asymptotic behavior

$$J(p,q;p_1) \sim -q^{-1/2} \theta(p_1 - p) \tag{4.16}$$

as $q \to \infty$ with p, p_1 fixed. It also has singularities on the axis, given by

$$J(p,q;p_1) \sim \pi^{-1} (p_1 - p)^{-1/2} \ln(p+q) \theta(p_1 - p) \tag{4.17}$$

as $(p+q) \to 0$. To eliminate the singularities on the axis, we add a solution of the cylindrical wave equation defined by the usual retarded integral for the flat-space wave equation in two spatial dimensions, with a source along the axis which compensates for the coefficient $\pi^{-1}(p_1 - p)^{-1/2}\theta(p_1 - p)$ of $\ln(p+q)$ in Eq. (4.17). This leads to the function

$$H(p,q;p_1) = J(p,q;p_1) + \frac{1}{\pi} \int_{-\infty}^{\min(2p_1, -2q)} \frac{d\xi}{(p_1 - \frac{1}{2}\xi)^{1/2} [(p - q - \xi)^2 - (p+q)^2]^{1/2}} . \tag{4.18}$$

The integral in Eq. (4.18) is elliptic. By standard methods it can be expressed in terms of Legendre functions, which can then be simplified with the help of quadratic transformation formulas for the hypergeometric function.[12] The simplest form for the resulting Green's function in the three different regions shown in Fig. 5 is

$$\begin{aligned} H(p,q;p_1) &= 0, \quad p < p_1 \\ &= (p+q)^{-1/2} P_{-1/2}(1 + 2(p_1 - p)/(p+q)), \quad p > p_1, \ q > -p_1 \\ &= |p_1 + q|^{-1/2} P_{-1/2}(1 - 2(p+q)/(p_1+q)), \quad p > p_1, \ q < -p_1 . \end{aligned} \tag{4.19}$$

We see that $J(p,q;p_1)$ has been precisely canceled in the region $\{p < p_1\}$ by the integral in Eq. (4.18). The Green's function $H(p,q;p_1)$ of Eq. (4.19) now satisfies all our requirements, since it is regular on the axis and obeys the differential equation (4.12) with the asymptotic behavior (4.13). Note that the "retarded" property that $H(p,q;p_1) = 0$ for $p < p_1$ is to be expected with our boundary conditions, by the usual energy conservation arguments for the wave equation, since there is no radiation input for H at $q = \infty$ when $p < p_1$.

We now define $A(p,q)$ by Eq. (4.14), and note that the integral converges since $h'(p_1)$ is $O((p_1)^{-2})$ as $p_1 \to -\infty$. It can be checked that $A(p,q)$ satisfies the Euler-Darboux equation (4.9) and the asymptotic condition (4.10), while being regular on the axis; uniqueness follows again by standard "energy" arguments.

Next we find E by integrating Eq. (4.7c). Since E should tend to zero rapidly as $X^3 = \gamma(z - j(t,0)) \to \infty$, when we match out into the nearly flat region ahead of the caustic region and of curved shock 1, we must have

$$E(X^1, X^2, X^3) = (j_\rho)^{-2} \int_{X^3}^{\infty} d\xi' \int_{\xi'}^{\infty} d\xi'' [(X^2)^{-2} A_{22}(X^1, X^2, \xi'') - (X^2)^{-3} A_2(X^1, X^2, \xi'')] . \tag{4.20}$$

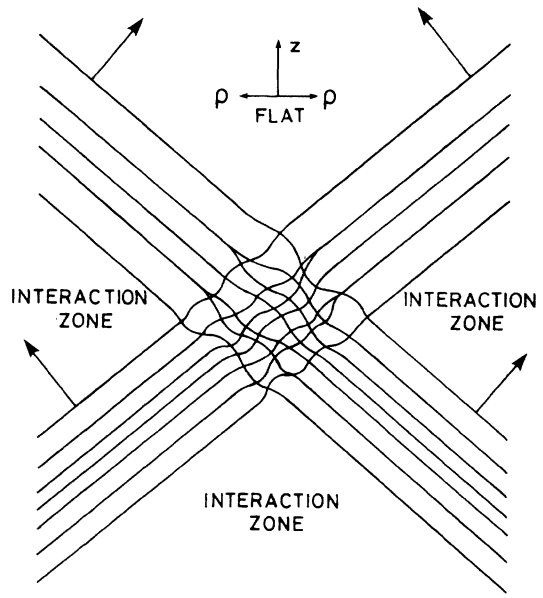

FIG. 6. Schematic diagram showing the caustic region produced as curved shock 1 crosses over itself near the symmetry axis, while moving upward into the flat spacetime region III. Distance along the axis is given by z, while ρ measures distance away from the axis in this representation of the instantaneous shock profile. The incoming shock 1 is shown in the top half of the diagram, separating the flat region III from the interaction zone IV, where the spacetime is strongly curved. As it moves in the arrowed direction, it undergoes a wavelike self-interaction in the center of the diagram. The shock re-forms and continues to move in the arrowed direction after its self-interaction, at the bottom of the diagram; however, the shock profile has been altered in the caustic region.

This expression for E also satisfies Eqs. (4.7b) and (4.7d), so that Eqs. (4.7a)–(4.7d) are consistent. We have now found completely the metric perturbations $\gamma^{-1/2}m_{ab}^{(1)}$ which give the dominant structure of the caustic region.

As a result of its wavelike self-interaction near the caustic region, the gravitational field has avoided producing a singularity, although the interaction in this region has managed to alter the profile of the curved shock. Beyond the caustic region, the curved shock continues traveling in almost a null direction, and lies within the interaction zone, so that we can no longer describe it analytically (see Fig. 6). This null direction corresponds in (p,q) coordinates to fixing q and letting $p\to\infty$. Thus, to find the modified profile, we should examine the "output" from our cylindrical wave equation, given the "input" specified by $h(p)$. The behavior of $A(p,q)$ as $p\to\infty$ with q fixed is not very revealing since A grows like const$\times p^{1/2}$ in this direction, because of the linear growth of $h(p)$ as $p\to\infty$. This is a gauge effect, produced since we are moving well behind the front of the incoming curved shock 1.

To see clearly the modification in the shock profile which takes place in the caustic region, we should examine instead the gauge-invariant leading curvature terms at $O(\gamma^{3/2})$. These curvature terms are essentially of five types (depending on the number of indices from the set $\{x,y\}$), which can all be written just in terms of A by using Eqs. (4.7a)–(4.7d). Examples of each type are

$$\begin{aligned}
&R_{tztz}=\tfrac{1}{2}\gamma^{3/2}(j_\rho)^2A_{33}+O(\gamma),\\
&R_{tztx}=-\tfrac{1}{2}\gamma^{3/2}x\rho^{-1}A_{23}+O(\gamma),\\
&R_{xzyz}=\tfrac{1}{2}\gamma^{3/2}[2+(j_\rho)^2]xy\rho^{-2}(j_\rho)^{-2}(A_{22}-A_2/\gamma\rho)\\
&\qquad+O(\gamma),\\
&R_{xyyz}=\tfrac{1}{2}\gamma^{3/2}x\rho^{-1}A_{23}+O(\gamma),\\
&R_{xyxy}=-\tfrac{1}{2}\gamma^{3/2}(j_\rho)^2A_{33}+O(\gamma).
\end{aligned}\tag{4.21}$$

Each of the leading curvature components satisfies a flat-space wave equation in two spatial dimensions with respect to the variables γx, γy, and $\gamma(z-j(t,0))$, since A satisfies such an equation [Eq. (4.7a)].

Consider for example the evolution of A_{33} in the caustic region, which then gives the components R_{tztz} and R_{xyxy}. The incoming data for A_{33} are

$$A_{33}\sim q^{-1/2}h'''(p),\tag{4.22}$$

as $q\to\infty$ with p fixed. Then

$$A_{33}(p,q)=\int_{-\infty}^{\infty}dp_1\,H(p,q;p_1)h'''(p_1).\tag{4.23}$$

We find the asymptotic behavior of $A_{33}(p,q)$ as $p\to\infty$ with q fixed from the corresponding behavior of $H(p,q;p_1)$ in Eq. (4.19). For this, we need the asymptotic expansion[13]

$$\begin{aligned}
P_{-1/2}(1+2\omega)&=\pi^{-1}[4\ln 2-\ln(1+\omega)]\\
&\quad+O((1+\omega)\ln(1+\omega))
\end{aligned}\tag{4.24}$$

as $\omega\to-1$. Hence the "output" for A_{33} is

$$A_{33}(p,q)\sim-\pi^{-1}p^{-1/2}\int_{-\infty}^{\infty}d\xi\,\ln|\xi|\,h'''(\xi-q),\tag{4.25}$$

as $p\to\infty$ with q fixed, where the coefficient of $p^{-1/2}\ln p$ vanishes since

$$\int_{-\infty}^{\infty}d\xi\,h'''(\xi)=0.\tag{4.26}$$

The integral in Eq. (4.25) can be evaluated, giving

$$A_{\xi\xi}\sim p^{-1/2}m(q)\tag{4.27}$$

as $p\to\infty$ with q fixed, where

$$m(q) = \frac{K_1}{\pi q}\left\{\frac{-2q^2(2q^2+5d^2)}{(q^2+d^2)^2} + \frac{3d^4 q}{(q^2+d^2)^{5/2}}\ln\left[\frac{(q^2+d^2)^{1/2}-q}{(q^2+d^2)^{1/2}+q}\right]\right\},$$
$$K_1 = 2^{5/2}\mu^{3/2}[1-16\mu^2/(\xi^2+\eta^2)]^{1/2} \times (\xi^2+\eta^2)^{-1}, \tag{4.28}$$
$$d^2 = (\xi^2+\eta^2)[1-16\mu^2/(\xi^2+\eta^2)]^{-2}.$$

Notice how the shock has been spread out during this self-interaction, since $m(q)$ decreases only as q^{-1} for large $|q|$, while the incoming profile $h''(p)$ decreases like p^{-3} at large $|p|$.

The other curvature terms behave in a similar way, where the field emerging behind the caustic region is given by

$$A_{23} \sim j_\rho p^{-1/2} m(q), \qquad (A_{22} - A_2/\gamma\rho) \sim (j_\rho)^2 p^{-1/2} m(q) \tag{4.29}$$

as $p \to \infty$ with q fixed.

We have now seen in some detail how the shock structure is modified in a region with linear dimensions of $O(\gamma^{-1})$ around the caustic region, where the curvature reaches the large size of $O(\gamma^{3/2})$, before the shock reemerges with altered profile, moving into the interaction zone. Had we instead examined the speed-of-light collision at $\gamma = \infty$, we would probably have encountered difficulties with a spacetime singularity at the caustic region, possibly accompanied by a Cauchy horizon along the continuation of the shock beyond the caustic region. The considerations of this section show that any such singularity must be of a fairly mild kind, since the shock has very similar structures both before and after it reaches the caustic region, and there should be a natural extension of the $\gamma = \infty$ spacetime through the impulsive shock continuation.

In the case of unequal masses, the statements in this section still hold when we replace γ by γ_1, if we are dealing (say) with the caustic region in curved shock 1.

V. WAVE GENERATION IN THE FAR-FIELD CURVED SHOCKS

So far, by considering the evolution of the curved shocks at distances of $O(1)$ away from the axis in the head-on collision, we have not seen any behavior which resembles that of radiation propagating out near future null infinity. The curved shock structure analyzed in Secs. III and IV may well eventually lead to a short burst of high-frequency radiation, which would carry a power of $O(1)$ in typical frequencies of $O(\gamma)$, giving a small total radiated energy of $O(\gamma^{-1})$ in the short time of $O(\gamma^{-1})$ that such radiation would last. But any calculation of this type of radiation would require us to follow the curved shocks beyond their caustic regions and into the interaction zone, where we are ignorant of the metric; our description of the curved shocks at ρ of $O(1)$ has not taken us out to the region where they are radiative.

However, the collision problem with γ large but finite has the desirable property that we can locate a region of each curved shock, where perturbation methods can be used to view the shock evolution all the way out to future null infinity. For shock 1 (say) this region is to be found at t values of $O(\gamma^2)$, ρ values of $O(\gamma)$, and $[z - j(t,\rho)]$ values of $O(1)$; thus we can perform radiation calculations by examining the curved shock near the surface $\{z = j(t,\rho)\}$ at large distances from the axis and at late times after the collision. We shall call this region the far-field curved shock 1.

There are various reasons for expecting behavior in the far-field curved shocks which is qualitatively different from that described in Sec. III for the curved shocks closer to the axis. First note that γ^2 is indeed a characteristic time for the far-field curved shock evolution, since the null geodesic generators of Eq. (3.3) have been deflected inward at the collision by an angle of $O(\gamma^{-1})$, approximately $8\mu/\rho$ in this region, and hence take a time of $O(\gamma^2)$ to reach the axis. This is further suggested by Eq. (3.19) giving the detailed evolution of shock 1 at ρ values of $O(1)$, where the evolution timescale grows like $(\xi^2+\eta^2)$ as $(\xi^2+\eta^2)$ becomes large. Note also that we consider $[z - j(t,\rho)]$ values of $O(1)$ in this region, rather than $[z - j(t,\rho)]$ values of $O(\gamma^{-1})$, in order to see the shock structure properly. For the incoming shock depends on $\hat{z}$ through quantities such as $[\hat{x}^2 + \hat{y}^2 + \gamma^2(\hat{z} - \beta\hat{t})^2]^{1/2}$, so that we have to alter $\hat{z}$ by amounts of $O(1)$ to move through the shock when $(\hat{x}^2 + \hat{y}^2)$ is of $O(\gamma^2)$; a similar statement should hold for the far-field shock after collision.

We can now see that the far-field curved shock structure must allow for the fact that the incoming velocity $\beta = 1 - \frac{1}{2}\gamma^{-2} + \cdots$ is not quite unity. For the curved shock should also progress with a velocity differing from 1 by an amount of $O(\gamma^{-2})$, and the cumulative effects of this velocity difference should alter the location of the shock in relation to $\{z = j(t,\rho)\}$ by an amount of $O(1)$ over the timescale of $O(\gamma^2)$. This effect should be visible in coordinates $\gamma^{-2}t$, $\gamma^{-1}\rho$, $[z - j(t,\rho)]$, and must be reflected in the governing partial differential equations.

We also see that the region where the shock generators focus near the axis at late times must be different from the caustic region described in

Sec. IV. For Eq. (3.3) shows that the vertical velocity of the caustic region in $\{z = j(t, \rho)\}$ is approximately $1 + 32\mu^2/(\xi^2 + \eta^2)$, only slightly above unity, when $(\xi^2 + \eta^2)$ is large. Hence, when $(\xi^2 + \eta^2)$ is of $O(\gamma^2)$, the excess velocity $32\mu^2/(\xi^2 + \eta^2)$ may be outweighed by the fact that the shock does not quite travel at the speed of light. So we should expect new qualitative features in the behavior of the far-field curved shocks near the axis, without the "spacelike" properties of a caustic region.

The far-field curved shock structure allows us to see gravitational radiation, provided we restrict attention to directions at angles of $O(\gamma^{-1})$ away from the z axis, for consider a null geodesic traveling at an angle θ of $O(\gamma^{-1})$. This geodesic will have reached ρ values of $O(\gamma)$ after a time of $O(\gamma^2)$, and $[z - j(t, \rho)]$ can remain of $O(1)$ along the geodesic over this period of time, since the z velocity will only differ from 1 by $O(\gamma^{-2})$. Thus we can observe the null geodesic for most of its way out to future null infinity, while remaining within far-field curved shock 1, which can be described by perturbation theory. In this way we can compute strong-field gravitational radiation using only perturbation methods.

As suggested by these remarks, the qualitative difference between the far-field curved shocks and the behavior described in Sec. III lies in the wavelike evolution of the far field, as compared to the geometrical optics of the shocks closer in. In the far-field shocks, there is enough time for transverse derivatives in the x and y directions to come into play, whereas only evolution along the rays is important while the shock is traveling from (ξ, η) values of $O(1)$ to the caustic region. The radiative behavior of the far-field curved shocks is produced when the wavelike incoming field (2.19) and (2.20) is distorted by the collision, so that the "waves" cease to represent a Schwarzschild field, and start to propagate in all directions. This idea of "virtual quanta" of gravitational radiation being made real by a collision was exploited by Matzner and Nutku[14] in a related calculation of gravitational waves generated by a high-speed encounter, in which a small mass passes a large mass with large impact parameter.

In analyzing the far-field curved shock 1, we prefer to use the variable $(z - t - 8\mu\ln\gamma)$ instead of $[z - j(t, \rho)]$. This simplifies the form of the field equations and is permissible since Eq. (3.3) shows

that

$$z - j(t, \rho) = (z - t - 8\mu\ln\gamma) - 8\mu\ln[\tfrac{1}{2}\gamma^{-1}\rho + (\tfrac{1}{4}\gamma^{-2}\rho^2 + 8\mu\gamma^{-2}t)^{1/2}] + 32\mu^2\gamma^{-2}t[\tfrac{1}{2}\gamma^{-1}\rho + (\tfrac{1}{4}\gamma^{-2}\rho^2 + 8\mu\gamma^{-2}t)^{1/2}]^{-2} + o(1) \tag{5.1}$$

as $\gamma \to \infty$, when regarded as a function of γ with $\gamma^{-2}t$, $\gamma^{-1}\rho$, and $(z - t - 8\mu\ln\gamma)$ fixed. Thus any function of $\gamma^{-2}t, \gamma^{-1}x, \gamma^{-1}y, [z - j(t, \rho)]$ can be rewritten as a function of $\gamma^{-2}t, \gamma^{-1}x, \gamma^{-1}y, (z - t - 8\mu\ln\gamma)$. Then we consider the asymptotic expansion for the metric in far-field curved shock 1:

$$g_{ab}(t, x, y, z, \gamma) = \eta_{ab} + \gamma^{-2}g^{(2)}_{ab}(\gamma^{-2}t, \gamma^{-1}x, \gamma^{-1}y, z - t - 8\mu\ln\gamma) + \gamma^{-3}g^{(3)}_{ab}(\gamma^{-2}t, \gamma^{-1}x, \gamma^{-1}y, z - t - 8\mu\ln\gamma) + \cdots \tag{5.2}$$

in the limit $\gamma \to \infty$ with $\gamma^{-2}t, \gamma^{-1}x, \gamma^{-1}y, (z - t - 8\mu\ln\gamma)$ fixed. We should also explain the omission of any term $\gamma^{-1}g^{(1)}_{ab}$ in Eq. (5.2). This arises from the form of the incoming shock at distances of $O(\gamma)$ from the axis:

$$g_{ab}(\hat{t}, \hat{x}, \hat{y}, \hat{z}, \hat{\gamma}) = \eta_{ab} + \gamma^{-2}j^{(2)}_{ab}(\gamma^{-1}\hat{x}, \gamma^{-1}\hat{y}, \hat{z} - \beta\hat{t}) + \gamma^{-3}j^{(3)}_{ab}(\gamma^{-1}\hat{x}, \gamma^{-1}\hat{y}, \hat{z} - \beta\hat{t}) + \cdots, \tag{5.3}$$

where the only nonzero components of $j^{(2)}_{ab}$ are

$$\begin{aligned} j^{(2)}_{\hat{x}\hat{x}} &= \gamma^{-2}(\hat{y}^2 - \hat{x}^2)f(\gamma^{-1}\hat{\rho}, \hat{z} - \beta\hat{t}), \\ j^{(2)}_{\hat{x}\hat{y}} &= -2\gamma^{-2}\hat{x}\hat{y}f(\gamma^{-1}\hat{\rho}, \hat{z} - \beta\hat{t}), \\ j^{(2)}_{\hat{y}\hat{y}} &= \gamma^{-2}(\hat{x}^2 - \hat{y}^2)f(\gamma^{-1}\hat{\rho}, \hat{z} - \beta\hat{t}), \end{aligned} \tag{5.4}$$

and the function f is defined in Eq. (2.16). The incoming far-field shock 1 will be distorted by the collision with shock 2, but the perturbation order γ^{-2} of the leading term will not be altered.

To find initial data for the far-field curved shock 1, we proceed as in Sec. III. There is a collision region where the two far-field shocks first meet, with

$$g_{ab}(\hat{t}, \hat{x}, \hat{y}, \hat{z}, \gamma) = \eta_{ab} + \gamma^{-2}n^{(2)}_{ab}(\hat{t}, \gamma^{-1}\hat{x}, \gamma^{-1}\hat{y}, \hat{z}) + \gamma^{-3}n^{(3)}_{ab}(\hat{t}, \gamma^{-1}\hat{x}, \gamma^{-1}\hat{y}, \hat{z}) + \cdots, \tag{5.5}$$

which is valid as $\gamma \to \infty$ and $\hat{t}, \gamma^{-1}\hat{x}, \gamma^{-1}\hat{y}, \hat{z} \to$ constants. Again there is the deceptive linearity of the term

$$n^{(2)}_{ab}(\hat{l}, \gamma^{-1}\hat{x}, \gamma^{-1}\hat{y}, \hat{z}) = j^{(2)}_{ab}(\gamma^{-1}\hat{x}, \gamma^{-1}\hat{y}, \hat{z} - \hat{l}) + j^{(2)}_{ab}(\gamma^{-1}\hat{x}, \gamma^{-1}\hat{y}, \hat{z} + \hat{l}), \quad (5.6)$$

where the shocks have in fact interacted since the coordinates $\hat{l}, \hat{x}, \hat{y}, \hat{z}$ are not Minkowskian behind shock 2. Using the coordinate transformation (2.3) just behind shock 2, we arrive at initial data for the far-field curved shock in the form (5.2), at $\gamma^{-2}t = 0$. The effect of the collision is only to give a logarithmic delay to the incoming shock 1; there is no extra contribution to $g^{(2)}_{ab}|_{\text{initial}}$ from the differential coordinate transformation behind shock 2 [the Lorentz transformation (2.8)], since this only differs from the identity by corrections of $O(\gamma^{-1})$ when $\hat{\rho}$ is of $O(\gamma)$. We find that the initial data

$$g^{(2)}_{ab}|_{\text{initial}} = g^{(2)}_{ab}(\gamma^{-2}t = 0, \gamma^{-1}x, \gamma^{-1}y, z - t - 8\mu\ln\gamma)$$

only have nonzero components:

$$\begin{aligned} g^{(2)}_{xx}|_{\text{initial}} &= \gamma^{-2}(y^2 - x^2) f(\gamma^{-1}\rho, z - t - 8\mu\ln\gamma - 8\mu\ln(\gamma^{-1}\rho)), \\ g^{(2)}_{xy}|_{\text{initial}} &= -2\gamma^{-2}xy f(\gamma^{-1}\rho, z - t - 8\mu\ln\gamma - 8\mu\ln(\gamma^{-1}\rho)), \\ g^{(2)}_{yy}|_{\text{initial}} &= \gamma^{-2}(x^2 - y^2) f(\gamma^{-1}\rho, z - t - 8\mu\ln\gamma - 8\mu\ln(\gamma^{-1}\rho)). \end{aligned} \quad (5.7)$$

One might expect this to act as characteristic initial data, since it refers to the state of the far-field curved shock 1 just behind the almost-null surface of shock 2.

Next consider the field equations for the far-field curved shock 1. To simplify the notation, we write

$$U = \gamma^{-2}t, \quad X = \gamma^{-1}x, \quad Y = \gamma^{-1}y, \quad V = z - t - 8\mu\ln\gamma, \quad P = (X^2 + Y^2)^{1/2}. \quad (5.8)$$

This anticipates our finding that "slow time" U and "distance through the shock" V both behave as null variables. For solving the field equations we again choose a special gauge; in the present context we use the symmetries of the problem to fix the gauge at all orders in perturbation theory:

$$\begin{aligned} &g_{tt} = -1 + H^1(U, P, V, \gamma), \quad g_{tx} = g_{ty} = 0, \\ &g_{tz} = H^2(U, P, V, \gamma), \\ &g_{xx} = 1 + (Y^2 - X^2)H^3(U, P, V, \gamma), \\ &g_{xy} = -2XYH^3(U, P, V, \gamma), \\ &g_{xz} = 0, \quad g_{yy} = 1 + (X^2 - Y^2)H^3(U, P, V, \gamma), \\ &g_{yz} = 0, \quad g_{zz} = 1 + H^4(U, P, V, \gamma), \end{aligned} \quad (5.9)$$

for some functions H^1, H^2, H^3, H^4. In particular, we have

$$\begin{aligned} &g^{(2)}_{tt} = A(U, P, V), \quad g^{(2)}_{tx} = g^{(2)}_{ty} = 0, \quad g^{(2)}_{tz} = C(U, P, V), \\ &g^{(2)}_{xx} = (Y^2 - X^2)E(U, P, V), \quad g^{(2)}_{xy} = -2XYE(U, P, V), \quad g^{(2)}_{xz} = 0, \\ &g^{(2)}_{yy} = (X^2 - Y^2)E(U, P, V), \quad g^{(2)}_{yz} = 0, \quad g^{(2)}_{zz} = G(U, P, V), \end{aligned} \quad (5.10)$$

for some functions A, C, E, G.

We consider first the (tt) component of the field equations, giving

$$A_{VV} + 2C_{VV} + G_{VV} = 0. \quad (5.11)$$

Since we require all perturbations to die out as we let $V \to +\infty$ and move well ahead of the curved shock, we find

$$A + 2C + G = 0. \quad (5.12)$$

The remaining field equations for $g^{(2)}_{ab}$ are

$$C_{PP} + C_P/P = -2P^4EE_{VV} - P^4E_VE_V, \quad (5.13a)$$

$$A_P + C_P = P^2E_P + 4PE, \quad (5.13b)$$

$$2E_{UV} + E_{PP} + 5E_P/P = 0. \quad (5.13c)$$

It is the last of these equations which determines the wavelike evolution of curved shock 1 at the leading order; Eq. (5.13c) shows that each of the "transverse" components $g^{(2)}_{xx}$, $g^{(2)}_{xy}$, and $g^{(2)}_{yy}$ obeys a flat-space wave equation with respect to the variables (U, X, Y, V). Having found E, one can use Eqs. (5.12), (5.13a), and (5.13b) to calculate A, C, and G; the boundary conditions are that A, C, and G should tend to zero as $P \to \infty$ with U, V fixed, and that they should be regular at $P = 0$. The boundary condition at large P should be imposed because the gravitational field tends to flatness at large radii, and the condition at small P arises since we are considering a one-parameter family of spacetimes which should each be smooth on the axis in the far-field curved shock (we saw in Sec. IV that the geometry is smooth around the axis in the shock region at early times, and there is no reason for this to change as the shock moves up the axis at later times).

Our initial data as presented in Eq. (5.7) are not compatible with Eqs. (5.13a) and (5.13b); i.e., they

are not part of a g_{ab} which satisfies the gauge conditions (5.9) to all orders in perturbation theory. This can be remedied by a gauge transformation which introduces nonzero components $g^{(2)}_{tt}$, $g^{(2)}_{tz}$, and $g^{(2)}_{zz}$, but does not alter $g^{(2)}_{xx}$, $g^{(2)}_{xy}$, and $g^{(2)}_{yy}$. Hence our characteristic initial data for Eq. (5.13c) on the "null surface" $\{U=0\}$ are

$$\begin{aligned} E(U=0, X, Y, V) &= f(P, V-8\mu\ln P) \\ &= 4\mu P^{-4}\{(V-8\mu\ln P) \\ &\quad -[P^2+(V-8\mu\ln P)^2]^{1/2}\} \\ &\quad +2\mu P^{-2}[P^2+(V-8\mu\ln P)^2]^{-1/2}. \end{aligned} \tag{5.14}$$

We must solve the equation

$$2\mathcal{E}_{UV}+\mathcal{E}_{XX}+\mathcal{E}_{YY}=0 \tag{5.15}$$

for $\mathcal{E}(U, X, Y, V)=e^{2i\phi}P^2E(U, P, V)$, subject to the initial condition (5.14) and a requirement that $\mathcal{E}\to 0$ rapidly when we let $V\to+\infty$ and move well ahead of the curved shock. Such characteristic initial-value problems are treated by Penrose,[15,16] and in our case the solution in $\{U>0\}$ is

$$\mathcal{E}(U, X, Y, V)=\frac{-1}{2\pi U}\int_0^\infty\int_0^{2\pi} dP'd\phi'P'\frac{\partial}{\partial V'} \times \mathcal{E}(0, X', Y', V') \tag{5.16}$$

where

$$X=P\cos\phi, \quad Y=P\sin\phi, \qquad X'=P'\cos\phi', \quad Y'=P'\sin\phi', \tag{5.17}$$

and V' is determined as a function of X', Y' by

$$V'=V+[P^2-2PP'\cos(\phi-\phi')+P'^2]/2U. \tag{5.18}$$

There is no difficulty with convergence in Eq. (5.16), since $(\partial/\partial V')\mathcal{E}(0, X', Y', V')\to 0$ as $P'\to 0$, and $(\partial/\partial V')\mathcal{E}(0, X', Y', V')$ is $O((P')^{-4})$ as $P'\to\infty$ with V' given by Eq. (5.18).

The dominant radiation field at angles of $O(\gamma^{-1})$ close to the axis is carried by the transverse metric components g_{xx}, g_{xy}, and g_{yy}. To find the radiation, we should move out to large distances in null directions. Thus we should examine the behavior of the gravitational field when $w\to\infty$ along the line

$$t=\tau+\gamma^2w-8\mu\ln\gamma, \quad x=\gamma\psi w\cos\phi, \quad y=\gamma\psi w\sin\phi, \quad z=(1-\gamma^{-2}\psi^2)^{1/2}\gamma^2w, \tag{5.19}$$

which becomes asymptotically null, in a direction at a small angle θ of approximately $\psi\gamma^{-1}$ from the axis. In (U, X, Y, V) coordinates this line becomes

$$U=w, \quad X=\psi w\cos\phi, \quad Y=\psi w\sin\phi, \quad V=-\tau-\tfrac{1}{2}\psi^2w, \tag{5.20}$$

disregarding corrections of higher order in γ^{-1}. The quantity τ gives the retarded time at future null infinity. From Eq. (5.16), we find

$$\begin{aligned} \mathcal{E}(U, X, Y, V) &= \frac{-\mu e^{2i\Phi}}{\pi w}\int_0^\infty P'dP'\int_0^{2\pi} e^{2i\Phi'}d\phi'(\psi P'\cos\phi'+\tau+8\mu\ln P') \\ &\quad \times\{[P'^2+(\psi P'\cos\phi'+\tau+8\mu\ln P')^2]^{-3/2}+2(P')^{-2}[P'^2+(\psi P'\cos\phi'+\tau+8\mu\ln P')^2]^{-1/2}\} \\ &\quad +e^{2i\Phi}\Lambda(\psi)w^{-1}+o(w^{-1}) \end{aligned} \tag{5.21}$$

as $w\to\infty$, where $\Lambda(\psi)$ is a function of ψ only and does not contribute to the radiation.

For a spacetime invariant under the symmetries $\phi\to\phi+\text{const}$ and $\phi\to-\phi$, the gravitational radiation is characterized by a real-valued function $c_\tau(\tau, \Theta)$ of retarded time and angle,[17] known as the "news function." This determines the rate of mass loss of an isolated gravitating system with these symmetries, due to emission of gravitational waves, according to

$$\frac{d(\text{mass})}{d\tau}=-\tfrac{1}{2}\int_0^\pi d\theta\sin\theta[c_\tau(\tau, \theta)]^2. \tag{5.22}$$

For our problem, the leading behavior of the news function at angles θ of $O(\gamma^{-1})$ is given by

$$c_\tau(\tau, \theta=\psi\gamma^{-1})=-\tfrac{1}{2}\lim_{w\to\infty}\left[w\frac{\partial}{\partial\tau}\mathcal{E}(U, X, Y=0, V)\right]+o(1) \tag{5.23}$$

as $\gamma\to\infty$, when regarded as a function of γ with τ and ψ fixed. Hence we find the news function

$$c_\tau(\tau, \theta=\psi\gamma^{-1})=\frac{3\mu}{2\pi}\int_0^\infty dP\int_0^{2\pi} d\phi\, P^3\cos 2\phi[P^2+(\psi P\cos\phi+\tau+8\mu\ln P)^2]^{-5/2}+o(1) \tag{5.24}$$

as $\gamma \to \infty$ with τ, ψ fixed. Allowing for higher-order corrections, the news function at angles of $O(\gamma^{-1})$ should be represented by an asymptotic expansion such as

$$c_\tau(\tau, \theta = \psi\gamma^{-1}) = \sum_{n=0}^{\infty} \gamma^{-n} Q_n(\tau, \psi), \tag{5.25}$$

of which we have so far calculated only $Q_0(\tau, \psi)$. There will be a similar expansion for angles of $O(\gamma^{-1})$ away from the backward direction $\theta = \pi$.

Note that we have managed in this way to calculate truly strong-field gravitational radiation, with power/solid angle of the typical size c^5/G, characteristic of fully nonlinear gravitational interactions, since there is no small scaling factor γ^{-n} in front of the leading term in Eq. (5.25). Although we used perturbation methods to analyze the small correction $\gamma^{-2} g^{(2)}_{ab}(\gamma^{-2}t, \gamma^{-1}x, \gamma^{-1}y, z - t - 8\mu \ln\gamma)$ to the flat-space metric in the far-field curved shock, the resulting radiation field includes terms behaving like $\gamma^{-2}/\gamma^{-2}(x^2+y^2+z^2)^{1/2}$ at large radii, which have lost their negative powers of γ. It has only been possible to calculate strong-field radiation in perturbation theory by exploiting the very special properties of the large-γ collision spacetimes. The underlying physical reason for the remarkable effectiveness of perturbation methods in this case seems to be that the waves in the far-field curved shock can escape out to future null infinity near the forward direction without being caught and overtaken by information from the highly nonlinear interaction zone; these waves are assisted in their escape by the logarithmic delay across shock 2, which allows them to set off with large positve values of z.

The integral in Eq. (5.24) is apparently not tractable analytically—only one variable can be integrated out. However, it can be computed numerically, and the results of computing $Q_0(\tau, \psi)$ as a function of τ for five different values of ψ are shown in Fig. 7. There is no need to recalculate $Q_0(\tau, \psi)$ for different energies μ, since μ simply provides a timescale for the radiation via

$$Q_0(\tau, \psi)\big|_{\text{energy } 1} = Q_0(\mu\tau - 8\mu \ln\mu, \psi)\big|_{\text{energy } \mu}.$$

As ψ is increased from zero, $Q_0(\tau, \psi)$ also changes slowly away from zero; this is to be expected for radiation in spacetimes which are axisymmetric, $\phi \to -\phi$ symmetric, and smooth near the axis.[17] For $\psi > 0$, $Q_0(\tau, \psi)$ always has two extrema and changes sign once, when regarded as a function of τ. As ψ is made larger, the amplitude grows and the pattern shifts to later and later retarded times, until the pattern stabilizes at a limiting shape,

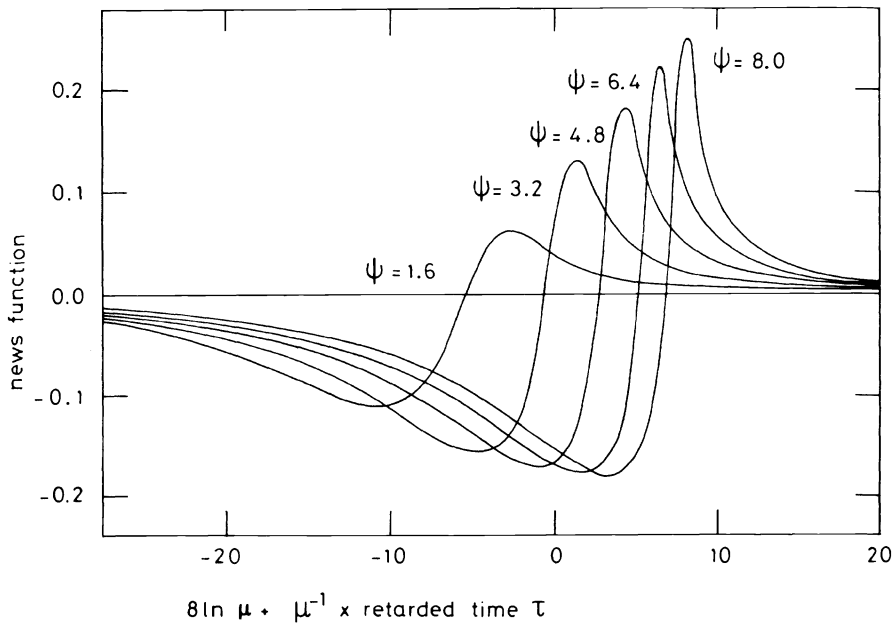

FIG. 7. The dominant news function, giving the amount of gravitational radiation emitted in a high-speed axisymmetric collision, at angles $\theta = \psi\gamma^{-1}$ close to the axis. Plotted horizontally is retarded time τ, measured in units of the energy μ of one incoming black hole. The square of the news function gives $(4\pi) \times$ power radiated/solid angle. The characteristic angular frequencies associated with the time interval between the minimum and maximum of the news function lie roughly in the range $0.3\,\mu^{-1}$–$0.6\,\mu^{-1}$, although lower frequencies are also important. As ψ is increased, the higher frequencies should gain in amplitude, since the time interval from minimum and maximum decreases and since the maximum grows into a higher and higher spike.

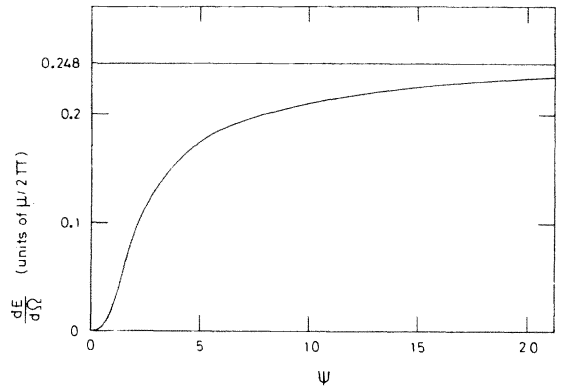

FIG. 8. Time-integrated power/solid angle in gravitational waves produced by a high-speed axisymmetric collision, at angles $\theta=\psi\gamma^{-1}$ close to the axis. On the vertical axis, energy/solid angle is measured in units of $\mu/2\pi$ in order to show the efficiency of the process in converting collision energy into gravitational waves; the units give the efficiency which the collision would have if the radiation were distributed isotropically with the news function seen at angle $\psi\gamma^{-1}$. At angles θ satisfying $\gamma^{-1}\ll\theta\ll1$, $dE/d\Omega$ will be close to the limiting value $0.248\,\mu/2\pi$. However, $dE/d\Omega$ may be different for larger values of θ.

with the exception of a narrow spike at the second peak, which continues to grow as $\psi\to\infty$. The time-integrated power/solid angle in $Q_0(\tau,\psi)$ is also plotted in Fig. 8; this rises monotonically from zero to a limit as $\psi\to\infty$. The limit is such that an energy $0.496\ \mu$ would be given out as gravitational radiation, if radiation were emitted isotropically over the whole celestial sphere with the limiting power/solid angle. In that case 24.8% of the original incoming energy 2μ would have been converted into gravitational waves. This is well below the 50% upper bound calculated by Penrose on the basis of the "cosmic censorship hypothesis," but still provides an estimate that the high-speed collision is an efficient generator of gravitational waves, removing a substantial fraction of the rest mass of the system.

This limiting behavior of the news function as $\psi\to\infty$ suggests that the radiation from the high-speed axisymmetric collision does not emerge in a beam near the axis, with angular width of $O(\gamma^{-1})$, as is familiar from the theory of distant encounters at large γ. Rather, $Q_0(\tau,\psi)$ apparently represents some detailed structure in the radiation on angular scales of $O(\gamma^{-1})$ near the axis, which should fit onto a radiation pattern spread over the whole celestial sphere, on angular scales of $O(1)$. Support for this view is provided by the recent work of Smarr.[18]

The limiting radiation pattern as $\psi\to\infty$ can be described analytically. As $\psi\to\infty$, $Q_0(\tau,\psi)$ becomes centered around the retarded time $\tau=8\mu\ln\psi$ (this can be traced to the logarithmic delay across shock 2), and the dominant contribution to the integral comes from P values of order ψ^{-1}. We write

$$\tau=8\mu\ln(\psi/\mu)+\tau',\quad P=\mu\psi^{-1}P', \tag{5.26}$$

and then consider

$$Q_0(\tau,\psi)=\frac{3\psi}{2\pi}\int_0^\infty dP'P'^3\int_0^{2\pi}d\phi\,\cos2\phi[P'^2+\psi^2(P'\cos\phi+8\ln P'+\tau'/\mu)^2]^{-5/2}. \tag{5.27}$$

For a given value of P', the main contribution from the angular integration arises from those ϕ values which minimize $(P'\cos\phi+8\ln P'+\tau'/\mu)^2$. If P' is such that $(P'\cos\phi+8\ln P'+\tau'/\mu)$ crosses zero, then the main contribution to the angular integral is produced by a narrow range of ϕ values, with width of order ψ^{-1}; the contribution to the whole integral from other P' values is suppressed. The angular integration can be performed, and we find the limit

$$Q_0(\tau=8\mu\ln(\psi/\mu)+\tau',\psi)\to-\frac{4}{\pi}\int_{\mathfrak{D}}\frac{dP'}{P'^2}\left[\frac{2(8\ln P'+\tau'/\mu)^2}{P'^2}-1\right]\times\left[1-\frac{(8\ln P'+\tau'/\mu)^2}{P'^2}\right]^{-1/2} \tag{5.28}$$

as $\psi\to\infty$ with τ' fixed ($\tau'/\mu\neq8-8\ln8$). Here the domain $\mathfrak{D}$ consists of those values P' such that

$$(8\ln P'-P'+\tau'/\mu)<0<(8\ln P'+P'+\tau'/\mu).$$

When $\tau'/\mu<8-8\ln8$, $\mathfrak{D}$ is one connected region, as in Fig. 9(a), but when $\tau'/\mu>8-8\ln8$, $\mathfrak{D}$ is in two disjoint pieces, as in Fig. 9(b). A graph of the limiting news function in Eq. (5.28) is shown in Fig. 10. The function has a logarithmic singularity at $\tau'/\mu=8-8\ln8$, which is mild in the sense that it only carries a finite amount of energy when we integrate the power across the singularity. As $\psi\to\infty$, the functions $Q_0(\tau,\psi)$, regarded as functions of τ, can only approximate the singular limiting news function by developing higher and higher spikes near $\tau'/\mu=8-8\ln8$.

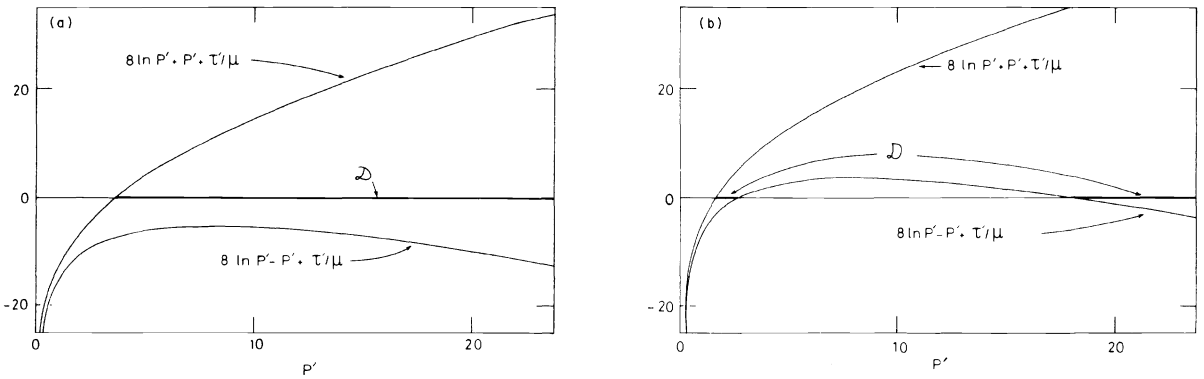

FIG. 9. (a) and (b) The domain $\mathfrak{D}$ of integration for Eq. (5.28), consisting of those numbers $P' > 0$ such that $8\ln P' - P' + \tau'/\mu < 0 < 8\ln P' + P' + \tau'/\mu$. In (a), $\tau'/\mu = -14.0 < 8 - 8\ln 8$, so that $\mathfrak{D}$ is one connected region. In (b), $\tau'/\mu = -5.0 > 8 - 8\ln 8$, and $\mathfrak{D}$ is in two disjoint pieces.

Let us consider further the radiation over angular scales of $O(1)$. This should be described by an asymptotic expansion of the form

$$c_{\tau'}(\tau', \theta) = \sum_{n=0}^{\infty} \gamma^{-n} S_n(\tau', \theta), \tag{5.29}$$

valid as $\gamma \to \infty$ with τ', θ fixed ($\theta \neq 0, \pi$), where the leading term $S_0(\tau', \theta)$ is precisely the news function for the collision at the speed of light. The functions $S_n(\tau', \theta)$ could only be calculated in their entirety by finding whole collision spacetimes, including their strong-field interaction zones. But we can obtain partial information on the $S_n(\tau', \theta)$ by using knowledge of the other expansion (5.25) for the one-parameter family of news functions, provided the two expansions match in an intermediate region near the axis where $\gamma^{-1} \ll \theta \ll 1$. Suppose, for example, that the one-parameter family

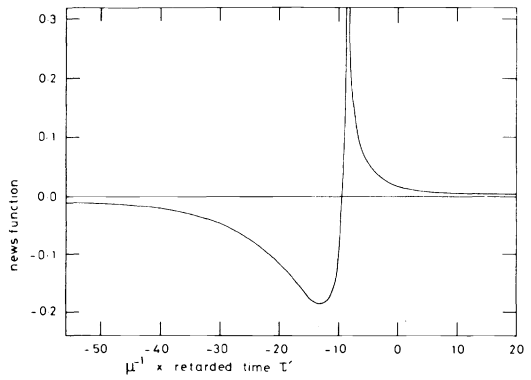

FIG. 10. The news function showing the gravitational radiation produced by a high-speed axisymmetric collision, at angles θ satisfying $\gamma^{-1} \ll \theta \ll 1$. This is found by taking the limit as $\psi \to \infty$ of the new function shown in Fig. 7. The peak has become infinitely high in this limit, with a logarithmic singularity; the time interval between trough and peak is approximately 4.5μ.

of news functions is so well behaved in a neighborhood of ($\gamma = \infty$, $\theta = 0$) that the news function can be expanded out in a double power series in γ^{-1} and θ (allowing both positive and negative powers of θ) valid in the intermediate region. This is consistent with our knowledge of $\gamma^0 Q_0(\tau, \psi)$, which provides the $\gamma^{-n}\theta^{-n}$ parts of the series via an expansion in negative powers of $\psi = \gamma\theta$ about $\psi = \infty$. In particular, the limiting news function of Eq. (5.28) gives the $\gamma^0\theta^0$ term, and hence should be just $S_0(\tau', \theta = 0)$. Thus, if these ideas of matching are correct, we can actually make an exact statement about the radiation field in the fully nonlinear spacetime formed by the axisymmetric collision of two black holes at the speed of light, while using only perturbation methods.

Provided we are correct in our identification of the limiting news function as $S_0(\tau', 0)$, we can make two remarks about the advantage of working with collisions at large but finite γ, rather than with impulsive wave collisions. First, note that the news function $S_0(\tau', \theta)$ will only be nonzero at $\theta = 0$ if the spacetime is not smooth on the axis near future null infinity.[17] Second, the logarithmic singularity in $S_0(\tau', \theta = 0)$ again implies that the $\gamma = \infty$ spacetime is, strictly speaking, not asymptotically flat; the impulsive shocks have focused each other so as to produce infinite radiative fields near future null infinity. Both remarks indicate that great care must be taken in any discussion which attempts to treat the $\gamma = \infty$ collision spacetime as a typical isolated radiating system, and that it can be understood more easily as a limit of the better-behaved finite-γ solutions.

If it is valid to match the two expansions for the news function as outlined above, then further information about $S_0(\tau', \theta)$ can be extracted by perturbation calculations of higher order $Q_n(\tau, \psi)$. This will be found from the $\gamma^0\theta^n = \gamma^{-n}\psi^n$ parts of

the news function, for $n>0$. Thus by calculating $Q_n(\tau,\psi)$ and matching out, one would find the θ^n part of $S_0(\tau',\theta)$. By this means, perturbation methods could be used to build up our knowledge of $S_0(\tau',\theta)$ near $\theta=0$. Since we are using a center-of-mass frame, $S_0(\tau',\theta)$ will be symmetrical about $\theta=\pi/2$, and (if sufficiently smooth) can be expanded as a convergent series

$$S_0(\tau',\theta)=\sum_{m=0}^{\infty} a_m(\tau')(\sin\theta)^m, \tag{5.30}$$

of which we have so far found only $a_0(\tau')$. The perturbation problem has the unusual feature that we can continue to gather important information by proceeding to high orders, since $\gamma^{-n-1}Q_{n+1}(\tau,\psi)$ can lead to an $a_{n+1}(\tau')$ at least as large as $a_n(\tau')$ found from the lower-order $\gamma^{-n}Q_n(\tau,\psi)$. But it may well be that $S_0(\tau',\theta)$ is dominated by the first few multipoles, so that it can be reconstructed accurately by carrying on our perturbation treatment to find the next few $a_m(\tau')$. For $n\geq 2$, the calculation of $Q_n(\tau,\psi)$ will start to involve the solution of inhomogeneous flat-space wave equations with complicated source terms, so that technical difficulties could become prohibitive in an attempt to find the angular structure of the $\gamma=\infty$ news function by this method.

It can in fact be shown that the angular expansion (5.30) for $S_0(\tau',\theta)$ involves only coefficients $a_m(\tau')$ for even m. This arises via matching, since the terms $\gamma^{-n}Q_n(\tau,\psi)$ in Eq. (5.25) are actually zero when n is odd. One can see this most easily by first carrying out the perturbation calculations in a different frame, where black hole 1 (having the low mass $M\gamma^{-1}$), is initially at rest before being struck by a large shock 2 with energy $M\gamma^{-1}(2\gamma^2-1)$. In this frame one has a problem in which the far field of black hole 1 is a weak perturbation on the strong nonlinear shock 2. This is essentially a situation with a small black hole in a background spacetime,[19] apart from modifications due to the fact that the "background spacetime" provided by shock 2 itself depends on the small parameter γ^{-1}. The initial far field of black hole 1 is partially converted into radiation when shock 2 passes, and the relevant field equations to describe this process involve perturbation theory with respect to the metric of shock 2. The perturbation theory can be phrased in a way which only involves even powers of γ^{-1}. For example, the initial field of black hole 1 depends on the variable $(M\gamma^{-1})/r = M\gamma^{-2}/(\gamma^{-1}r)$, which scales as γ^{-1} in the region under consideration, where $\gamma^{-1}r$ is of $O(1)$. The even powers of γ^{-1} in the incoming field of shock 2 arise from the γ^2 in the ratio energy/mass $=2\gamma^2-1$. Finally, by transforming back to the original frame, one finds that the asymptotic expansion (5.25) takes the form

$$c_\tau(\tau,\theta=\psi\gamma^{-1})=\sum_{n=0}^{\infty}\gamma^{-2n}Q_{2n}(\tau,\psi). \tag{5.31}$$

Hence, if it is valid to match the expansions for the news function in the manner suggested, Eq. (5.30) should be replaced by

$$S_0(\tau',\theta)=\sum_{m=0}^{\infty} a_{2m}(\tau')(\sin\theta)^{2m}. \tag{5.32}$$

In particular, a calculation to the next nontrivial order in perturbation theory would yield $a_2(\tau')$ after matching out $Q_2(\tau,\psi)$; this calculation would require us to solve a flat-space wave equation in $\{U>0\}$ with a source quadratic in the lowest-order perturbations of flat space.

When the black-hole masses are unequal, the only modification to the radiation field near the axis is that γ should be replaced by γ_1 near the forward direction ($\theta=0$) and by γ_2 near the backward direction ($\theta=\pi/2$). For example, $c_\tau(\tau,\theta=\psi/\gamma_1)=Q_0(\tau,\psi)+O(\gamma^{-2})$. Since only the energy μ determines the radiation for the $\gamma=\infty$ collision on angular scales of $O(1)$, the leading term $S_0(\tau',\theta)$ in Eq. (5.29) will be unchanged; however, the functional form of $S_n(\tau',\theta)$ for $n>0$ may be different.

VI. THE NONAXISYMMETRIC CASE

The methods used to describe the curved shocks and wave generation in the previous three sections can also be applied to those spacetimes formed by nonaxisymmetric collisions or encounters of black holes moving at nearly the speed of light. As in the axisymmetric problem, the spacetimes will again possess curved shock regions which can be analyzed using perturbation methods.

There is a wide range of possibilities available, since we now have the freedom of scaling the impact parameter while considering a one-parameter family of spacetimes labeled by the small parameter γ^{-1}. First consider the scaling (impact parameter)$\to$constant as $\gamma\to\infty$, which would describe a situation where the impact parameter is of a size comparable with the energy μ. Then the limiting $\gamma=\infty$ spacetime will be quite different from the axisymmetric $\gamma=\infty$ spacetime of the preceding section, and the radiation heading out at angles θ of $O(1)$ will also differ from the axisymmetric radiation described by Eq. (5.29). The nonaxisymmetric gravitational radiation will be characterized by a complex news function[20] $c_{\tau'}(\tau',\theta,\phi)$, having an asymptotic expansion

$$c_{\tau'}(\tau',\theta,\phi)=\sum_{n=0}^{\infty}\gamma^{-n}S_n(\tau',\theta,\phi), \tag{6.1}$$

where the leading term $S_0(\tau', \theta, \phi)$ gives the strong-field gravitational radiation produced in the interaction zone of the $\gamma = \infty$ spacetime. There will also be some detailed structure in the radiation on angular scales of $O(\gamma^{-1})$ near the axis, given by an asymptotic expansion

$$c_\tau(\tau, \theta = \psi\gamma^{-1}, \phi) = \sum_{n=0}^{\infty} \gamma^{-n} Q_n(\tau, \psi, \phi), \tag{6.2}$$

where the successive terms could be calculated by examining in greater and greater detail the structure of the far-field curved shock 1. However, by contrast with the radiation (6.1) on angular scales of $O(1)$, we find that the leading term $Q_0(\tau, \psi, \phi)$ is identical with the leading term $Q_0(\tau, \psi)$ of Eq. (5.25) for the radiation close to the axis in the axisymmetric problem. This arises since the structure of the far-field curved shock 1 is again found by solving a characteristic initial-value problem behind shock 2, and the displacement of the initial data by distances of $O(1)$ in the x and y directions, produced by the nonzero impact parameter, does not alter the perturbation fields $g_{xx}^{(2)}$, $g_{xy}^{(2)}$, and $g_{yy}^{(2)}$. The nonzero impact parameter only produces higher-order effects in this region since the displacement is small by comparison with the $O(\gamma)$ length scales in the x and y directions, appropriate to the far-field shock structure. If matching of the two expansions for the news function is permissible, then we find that $S_0(\tau', \theta = 0, \phi)$ is just the limiting news function of Eq. (5.28), regardless of the value of the impact parameter. Higher-order calculations in the curved shock and matching would then enable us to reconstruct more details of the angular structure of $S_0(\tau', \theta, \phi)$, in the same way as suggested for the axisymmetric problem in the preceding section.

The impact parameter can also be scaled up as $\gamma \to \infty$, so that we can describe a one-parameter family of spacetimes in which the black holes undergo a fairly distant encounter, rather than a collision or close encounter. The scaling which treats the impact parameter as $O(\gamma)$ is of particular interest, and will be the subject of the remainder of this section. Thus we shall consider the case

$$\text{impact parameter} = b\gamma, \tag{6.3}$$

where b is a positive constant. Recall that the mass M is scaled as $\mu\gamma^{-1}$, so that the impact parameter is now treated as $O(M\gamma^2)$. We have chosen this scaling because the interaction of the black holes will be sufficiently weak that the whole spacetime can now be described using perturbation methods; but the encounter is still sufficiently close that it generates strong radiation, which could not be calculated by the more usual perturbation techniques applied to the bremsstrahlung problem.

We can distinguish at least four different types of gravitational radiation generated by such an encounter; each type of radiation will need a separate asymptotic expansion for its description, and the expansions should match on the various overlap regions where one type of radiation merges into another. This situation is depicted in Fig. 11, which shows the spatial regions containing different types of radiation, at a time of $\frac{1}{4}b\gamma$ after the shocks have passed through each other.

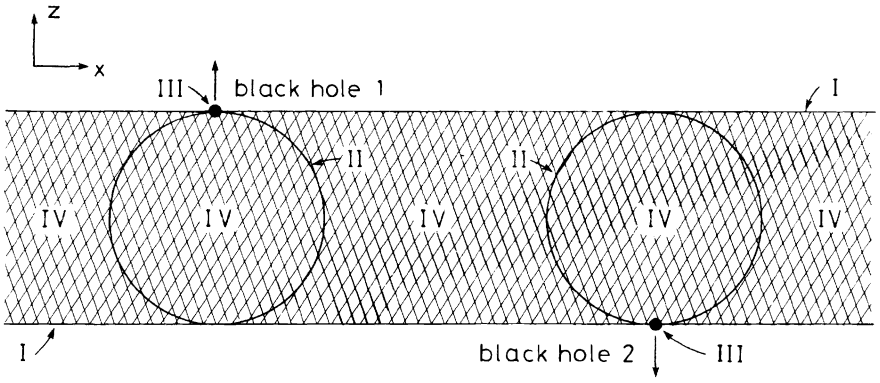

FIG. 11. A high-speed encounter with impact parameter $b\gamma$ leads to a variety of types of gravitational radiation, generated in different parts of the spacetime. The various different regions are seen here in the plane of motion of the black holes, at a time $\frac{1}{4}b\gamma$ after the shocks have met. The dominant beamed part of the radiation is produced in the far-field shocks (I), which are just beginning to evolve after their collision. Weak radiation is generated at distances of $O(1)$ from each black hole as it passes through the other shock, and propagates out in all directions (II). High-frequency beamed radiation generated at distances of $O(\gamma^{-1})$ from each black hole is still close to the holes, in the regions III. Region IV contains weak low-frequency radiation, left in the wake of the shocks.

First, there will be radiation near the axis, generated by the collision of the far-field shocks at distances of $O(\gamma)$ away from the black holes; this radiation will have structure on angular scales of $O(\gamma^{-1})$ close to the forward and backward directions. If we fix our attention on angles $\theta = \psi\gamma^{-1}$ of $O(\gamma^{-1})$ close to the forward direction, then the news function and the radiation time scale are both of $O(1)$, when $\gamma \to \infty$. Thus the radiation near the axis again carries power/solid angle of the size c^5/G characteristic of fully nonlinear interactions. But this intensity is now spread only over a solid angle of $O(\gamma^{-2})$, since for $b > 0$ the radiation is beamed, as might be expected in a fairly distant encounter at large γ. This type of radiation carries the bulk of the energy emitted to future null infinity, and will be discussed in more detail below.

Second, there will be radiation generated at distances of $O(1)$ away from black hole 2 when it passes through shock 1, and also at distances of $O(1)$ away from black hole 1 when it passes through shock 2; this travels outward in the regions denoted by II in Fig. 11. The part of shock 1 through which black hole 2 passes can be approximated by a weak plane wave (not just a plane-fronted wave). Then the radiation is produced in the scattering of this weak wave by the strong plane-fronted shock 2 at distances of $O(1)$ from black hole 2. Thus it is calculated by means of perturbation theory in a plane-fronted shock background. Expressions for this radiation have been found by the author, although they are not written down here. The radiation is to be found at all angles θ, and the news function in this region scales as $O(\gamma^{-2})$ with a timescale of $O(1)$ when we fix $\theta(\neq 0$ or $\pi)$ and let $\gamma \to \infty$; it carries only a negligible fraction of the total energy emitted.

Third, another type of radiation will be generated at distances of $O(\gamma^{-1})$ away from black hole 2 when it passes through shock 1, and similarly at distances of $O(\gamma^{-1})$ away from black hole 1 when it passes through shock 2. The gravitational field at distances of $O(\gamma^{-1})$ away from black hole 2 (say) cannot be accurately represented by a plane-fronted wave; instead one must take account of the details of the Schwarzschild geometry on the length scales of $O(M) = O(\gamma^{-1})$ comparable with the radius of the event horizon. The radiation generated in this region is most easily calculated by working in the rest frame of black hole 2. In this frame, the approaching shock 1 will again resemble a plane wave, and the Riemann curvature of shock 1 will be much less than the $O(\gamma^2)$ Riemann curvature of black hole 2 on these length scales. Thus the radiation should be calculated from the scattering of weak plane gravitational waves in a Schwarzschild background; this is discussed, for example, by Chrzanowski, Matzner, Sandberg, and Ryan.[21] There will not be a simple analytical form for the resulting scattered radiation, since the incoming plane waves must be Fourier-analyzed and decomposed into angular harmonics before the scattering is found mode by mode. When we boost back into the center-of-mass frame, we find that this radiation is beamed, with structure on angular scales of $O(\gamma^{-1})$, close to $\theta = \pi$. The news function scales as $O(1)$, and the time scale for the radiation is $O(\gamma^{-2})$. Thus the radiation from this region attains a large power/solid angle for a very brief time. To an observer situated at a large radius, near $\theta = \pi$, this radiation will appear as some rapid variations superimposed on the much smoother news function generated in the far-field curved shock 2. In Fig. 11, this radiation is to be found in the regions denoted by III; it has not yet had time to move far from the black holes.

Fourth, there will be some radiation with longer wavelengths of $O(\gamma)$, comparable with the impact parameter $b\gamma$. Like the strong radiation in the far-field curved shocks, it will be generated by the collision of the incoming shocks at distances of $O(\gamma)$ from the black holes; but unlike that radiation, it travels out at all angles θ of $O(1)$. It can be found by working with the expansion

$$g_{ab}(t, x, y, z, \gamma) = \eta_{ab} + \gamma^{-2} f^{(2)}_{ab}(\gamma^{-1}t, \gamma^{-1}x, \gamma^{-1}y, \gamma^{-1}z) + \cdots \tag{6.4}$$

appropriate to the structure of the field in region IV of Fig. 11, at t, x, y, z values of $O(\gamma)$. The leading term $\gamma^{-2} f^{(2)}_{ab}$ is calculated from the scattering of two weak impulsive plane-fronted waves; such a scattering has been discussed by Curtis.[6] The news function is of $O(\gamma^{-2})$ over the timescale of $O(\gamma)$, characteristic of this radiation, and so the energy carried by such radiation is small compared to the energy in the beams.

We now return to the most important part of the radiation, generated in the far-field curved shocks. Just as in the axisymmetric case, the detailed structure of the far-field curved shock 1 will be given by an asymptotic expansion

$$g_{ab}(t, x, y, z, \gamma) = \eta_{ab} + \gamma^{-2} g^{(2)}_{ab}(\gamma^{-2}t, \gamma^{-1}x, \gamma^{-1}y, z - t - 8\mu \ln\gamma) + \gamma^{-3} g^{(3)}_{ab}(\gamma^{-2}t, \gamma^{-1}x, \gamma^{-1}y, z - t - 8\mu \ln\gamma) + \cdots . \tag{6.5}$$

If we also use the previous notation

$$U=\gamma^{-2}t,\quad X=\gamma^{-1}x,\quad Y=\gamma^{-1}y,$$
$$V=z-t-8\mu\ln\gamma, \tag{6.6}$$

then we again find that the "transverse" components $g^{(2)}_{xx}$, $g^{(2)}_{xy}$, and $g^{(2)}_{yy}$, which determine the leading radiation field near the axis, satisfy flat-space wave equations

$$2g^{(2)}_{xx,UV}+g^{(2)}_{xx,XX}+g^{(2)}_{xx,YY}=0,$$
$$2g^{(2)}_{xy,UV}+g^{(2)}_{xy,XX}+g^{(2)}_{xy,YY}=0, \tag{6.7}$$
$$2g^{(2)}_{yy,UV}+g^{(2)}_{yy,XX}+g^{(2)}_{yy,YY}=0.$$

The characteristic initial data at the "null surface" $\{U=0\}$ are found as in Sec. V by following shock 1 as it passes through shock 2. Thus suppose that the coordinates are arranged to make the incoming black hole 1 approach with $x=-b\gamma$, $y=0$ at early times, while black hole 2 initially has $x=0$, $y=0$. The only effect of shock 2 on the dominant structure of shock 1 is to displace the incoming data along the generators of the characteristic initial surface. This leads to

$$g^{(2)}_{xx}(U=0,X,Y,V)=[Y^2-(X+b)^2]\,f([(X+b)^2+Y^2]^{1/2},\ V-4\mu\ln(X^2+Y^2)),$$
$$g^{(2)}_{xy}(U=0,X,Y,V)=-2(X+b)Y\,f([(X+b)^2+Y^2]^{1/2},\ V-4\mu\ln(X^2+Y^2)),$$
$$g^{(2)}_{yy}(U=0,X,Y,V)=[(X+b)^2-Y^2]\,f([(X+b)^2+Y^2]^{1/2},\ V-4\mu\ln(X^2+Y^2)), \tag{6.8}$$

where f is the function defined in Eq. (2.16). The scaling of the impact parameter as $b\gamma$ has been designed to make an appreciable alteration to the characteristic initial data of Eqs. (5.10), (5.14) and hence to the structure of the radiation on angular scales of $O(\gamma^{-1})$ close to the axis.

The characteristic initial data (6.8) demonstrate a significant difference between the axisymmetric collision problem and the encounter with $b>0$. Since the leading Riemann curvature at $O(\gamma^{-2})$ is linear in $\partial^2 g^{(2)}_{xx}/\partial V^2$, $\partial^2 g^{(2)}_{xy}/\partial V^2$, and $\partial^2 g^{(2)}_{yy}/\partial V^2$, and since

$$\partial^2 f(p,q)/\partial q^2=-6\mu(p^2+q^2)^{-5/2}, \tag{6.9}$$

we see that the leading curvature terms become singular at $X=-b$, $Y=0$, $V=8\mu\ln b$ when $b>0$, but that they have no singularities at finite X, Y, V on the initial surface when $b=0$. On the other hand, the $O(\gamma^{-2})$ curvature terms die away like $(X^2+Y^2+V^2)^{-3/2}$ as we move off to infinity in any direction on the initial surface when $b>0$, whereas the curvature grows indefinitely as we let $V\to-\infty$ and stay close to $X=0$, $Y=0$ in the axisymmetric problem. Thus the singularity appearing at $X=-b$, $Y=0$, $V=8\mu\ln b$, where black hole 1 emerges through shock 2, has been pushed to $V=-\infty$ by the infinite logarithmic delay when $b=0$. It was this behavior of the initial data at large negative V which made the news function tend to a limiting shape as $\psi\to\infty$ in Sec. V, showing that the radiation in the axisymmetric problem is not beamed. In the nonaxisymmetric problem with $b>0$, we shall find that the radiation is beamed, with the leading term in the news function tending to zero as $\psi\to\infty$, because of the rapid decrease of the initial curvature as $X^2+Y^2+V^2\to\infty$.

In Sec. V there was no need to consider the motion of black hole 1 after it hits shock 2, because of the infinite delay, but here for $b>0$ we must subtract out the singular part of the initial data representing the nonradiative far field of black hole 1, which continues to travel almost in the z direction behind shock 2. To find this part of the initial data, note that black hole 1 will move essentially along a geodesic of the gravitational field produced by black hole 2, using arguments as in Ref. 19. Hence for our purposes we can regard black hole 1 as moving along a straight line before and after it passes through shock 2, with the deflection in the line found from the geodesic equation in an impulsive shock background. The incoming line is given by

$$X=-b,\quad Y=0,\quad z=(1-\tfrac{1}{2}\gamma^{-2})t, \tag{6.10}$$

and hence the outgoing line is

$$X=-b+8\mu t/b\gamma^2,$$
$$Y=0, \tag{6.11}$$
$$z=(1-\tfrac{1}{2}\gamma^{-2}-32\mu^2/b^2\gamma^2)t+8\mu\ln(b\gamma),$$

disregarding corrections of higher order in γ^{-1}. Thus black hole 1 has been deflected by an angle of approximately $8\mu/b\gamma$ due to the attraction of the other black hole, and it remains in the region of the far-field curved shock thereafter, since X, Y, and $(z-t-8\mu\ln\gamma)$ remain of $O(1)$ when t is of $O(\gamma^2)$ in Eq. (6.11). In (U,X,Y,V) coordinates the outgoing line is

$$X=-b+8\mu U/b,$$
$$Y=0, \tag{6.12}$$
$$V=8\mu\ln b-(\tfrac{1}{2}+32\mu^2/b^2)U,$$

with $U\geq 0$.

By considering the incoming field (5.3) and (5.4) of black hole 1, we can find the solutions of the wave equation which represent a boosted Schwarzschild field with no radiation, where the black hole moves along the line $X=0$, $Y=0$, $V=-\frac{1}{2}U$. These are just

$$g^{(2)}_{xx}(U,X,Y,V) = -g^{(2)}_{yy}(U,X,Y,V) = (Y^2 - X^2) f((X^2+Y^2)^{1/2}, V + \tfrac{1}{2}U),$$
$$g^{(2)}_{xy}(U,X,Y,V) = -2XY f((X^2+Y^2)^{1/2}, V + \tfrac{1}{2}U). \tag{6.13}$$

By constructing a Poincaré transformation in the (U,X,Y,V) space which maps the line $X=0, Y=0$, $V=-\frac{1}{2}U$ into the line (6.12), we arrive at the solutions which represent the uniform motion of black hole 1 in $\{U>0\}$:

$$g^{(2)}_{xx}(U,X,Y,V) = -g^{(2)}_{yy}(U,X,Y,V)$$
$$= [Y^2 - (X+b-8\mu U/b)^2] f([(X+b-8\mu U/b)^2+Y^2]^{1/2}, V + \tfrac{1}{2}U - 32\mu^2 U b^{-2} + 8\mu X b^{-1} + 8\mu - 8\mu \ln b),$$
$$g^{(2)}_{xy}(U,X,Y,V) = -2(X+b-8\mu U/b)Y \tag{6.14}$$
$$\times f([(X+b-8\mu U/b)^2+Y^2]^{1/2}, V + \tfrac{1}{2}U - 32\mu^2 U b^{-2} + 8\mu X b^{-1} + 8\mu - 8\mu \ln b).$$

Since we only wish to calculate the radiation generated by the passage of shock 1 through shock 2, these solutions must be subtracted off from the complete $g^{(2)}_{xx}$, $g^{(2)}_{xy}$, and $g^{(2)}_{yy}$. This leaves us with the initial data

$$g^{(2)}_{xx}(U=0,X,Y,V) = -g^{(2)}_{yy}(U=0,X,Y,V)$$
$$= [Y^2 - (X+b)^2]\{ f([(X+b)^2+Y^2]^{1/2}, V - 4\mu \ln(X^2+Y^2))$$
$$- f([(X+b)^2+Y^2]^{1/2}, V + 8\mu X b^{-1} + 8\mu - 8\mu \ln b)\},$$
$$g^{(2)}_{xy}(U=0,X,Y,V) = -2(X+b)Y\{ f([(X+b)^2+Y^2]^{1/2}, V - 4\mu \ln(X^2+Y^2)) \tag{6.15}$$
$$- f([(X+b)^2+Y^2]^{1/2}, V + 8\mu X b^{-1} + 8\mu - 8\mu \ln b)\}$$

for the radiative part of the field. These initial data are somewhat better behaved than those in Eq. (6.8), since the curvature again decreases like $(X^2+Y^2+V^2)^{-3/2}$ as $X^2+Y^2+V^2 \to \infty$ on the initial surface, but now the curvature only grows like $[(X+b)^2+Y^2+(V-8\mu \ln b)^2]^{-1/2}$ as the point $X=-b$, $Y=0$, $V=8\mu \ln b$ is approached. Correspondingly, the first derivatives $\partial g^{(2)}_{xx}/\partial V$, $\partial g^{(2)}_{xy}/\partial V$, and $\partial g^{(2)}_{yy}/\partial V$ are now bounded on the surface $\{U=0\}$.

The solutions of the flat-space wave equation with these characteristic initial data can be found as in Sec. V by using the representation (5.16); we are requiring, as before, that $g^{(2)}_{xx}$, $g^{(2)}_{xy}$, and $g^{(2)}_{yy}$ tend to zero rapidly when we let $V \to +\infty$ and move well ahead of the far-field curved shock 1. The dominant behavior as $\gamma \to \infty$ of the complex news function $c_\tau(\tau, \theta = \psi\gamma^{-1}, \phi)$, characterizing the gravitational radiation near the axis, is again found by considering $g^{(2)}_{xx}$, $g^{(2)}_{xy}$, and $g^{(2)}_{yy}$ as $w \to \infty$ with

$$U = w, \quad X = \psi w \cos\phi, \quad Y = \psi w \sin\phi,$$
$$V = -\tau - \tfrac{1}{2}\psi^2 w. \tag{6.16}$$

Using the definition of the news function in Ref. 20, we find

$$c_\tau(\tau, \theta = \psi\gamma^{-1}, \phi) = \tfrac{1}{2} e^{-2i\phi} \lim_{w\to\infty} \left[w \left(\frac{\partial g^{(2)}_{xx}}{\partial \tau} + i \frac{\partial g^{(2)}_{xy}}{\partial \tau} \right) \right]$$
$$+ O(\gamma^{-1}) \tag{6.17}$$

as $\gamma \to \infty$ with τ, ψ, ϕ fixed. Hence $\partial g^{(2)}_{xx}/\partial\tau$ and $\partial g^{(2)}_{xy}/\partial\tau$ provide the leading term $Q_0(\tau,\psi,\phi)$ of an expansion of the form (6.2) describing the radiation near $\theta = 0$. For a nonaxisymmetric problem, the news function then determines the rate of mass loss in gravitational waves at retarded time τ according to

$$\frac{d(\text{mass})}{d\tau} = \frac{-1}{4\pi} \int_0^\pi d\theta \int_0^{2\pi} d\phi \, \sin\theta \, |c_\tau(\tau,\theta,\phi)|^2. \tag{6.18}$$

From Eq. (6.15) and the representation (5.16), we obtain the asymptotic behavior of $\partial g^{(2)}_{xx}/\partial\tau$ and $\partial g^{(2)}_{xy}/\partial\tau$ needed for the calculation of $Q_0(\tau,\psi,\phi)$:

$$\frac{\partial g^{(2)}_{xx}}{\partial \tau} \sim \frac{3\mu}{\pi w} \int_{-\infty}^{\infty}\int_{-\infty}^{\infty} dX\, dY [(X+b)^2 - Y^2]$$
$$\times (\{(X+b)^2 + Y^2 + [\tau + X\psi\cos\phi + Y\psi\sin\phi + 4\mu \ln(X^2+Y^2)]^2\}^{-5/2}$$
$$- [(X+b)^2 + Y^2 + (\tau + X\psi\cos\phi + Y\psi\sin\phi - 8\mu b^{-1} X + 8\mu \ln b - 8\mu)^2]^{-5/2}), \tag{6.19a}$$

$$\frac{\partial g_{xy}^{(2)}}{\partial \tau} \sim \frac{6\mu}{\pi w}\int_{-\infty}^{\infty}\int_{-\infty}^{\infty} dX\,dY(X+b)Y$$

$$\times \left(\left\{(X+b)^2+Y^2+\left[\tau+X\psi\cos\phi+Y\psi\sin\phi+4\mu\ln(X^2+Y^2)\right]^2\right\}^{-5/2}\right.$$

$$\left.-\left[(X+b)^2+Y^2+(\tau+X\psi\cos\phi+Y\psi\sin\phi-8\mu b^{-1}X+8\mu\ln b-8\mu)^2\right]^{-5/2}\right) \qquad (6.19b)$$

as $w\to\infty$.

It can be shown that the second term,

$$\left[(X+b)^2+Y^2+(\tau+X\psi\cos\phi+Y\psi\sin\phi\right.$$

$$\left.-8\mu b^{-1}X+8\mu\ln b-8\mu)^2\right]^{-5/2},$$

in the heavy parentheses of Eqs. (6.19a) and (6.19b) does not actually contribute to the integrals, provided $\tau\neq b\psi\cos\phi-8\mu\ln b$. This term has appeared because we subtracted out the initial data for Eq. (6.14), representing the boosted Schwarzschild field of black hole 1 after the encounter. Its only role is to ensure that the integrals (6.19a) and (6.19b) are well behaved near $\tau=b\psi\cos\phi-8\mu\ln b$, the retarded time at which future null infinity is intersected by the future null cone of the point $(U=0, X=-b, Y=0, V=8\mu\ln b)$, where black hole 1 has just emerged through shock 2.

To obtain more detailed understanding of this radiation, one should compute the integrals (6.19a) and (6.19b) numerically. So far this has not been carried out because of the amount of computation required. An accurate calculation of the news function for just one value of the parameter b/μ would involve computing two integrals for a range of values of the three quantities (τ,ψ,ϕ), rather than only the one integral depending on the two parameters (τ,ψ), computed in the case $b=0$.

However, the integrals (6.19a) and (6.19b) do permit us to see that the radiation is beamed when $b>0$, so that the strong-field intensity, carrying power/solid angle comparable with c^5/G, only reaches out to θ values of $O(\gamma^{-1})$. For as $\psi\to\infty$, we find that the leading term $Q_0(\tau,\psi,\phi)$ decreases like ψ^{-2}. When ψ is large, the main contribution to the integrals comes from the region where X and Y are of order ψ^{-1}. By transforming to integration variables $X\psi$, $Y\psi$ one obtains

$$Q_0(\tau,\psi,\phi)=\frac{3\mu b^2 e^{-2i\phi}}{2\pi\psi^2}\int_{-\infty}^{\tau}d\tau'\int_0^{\infty}\rho\,d\rho\int_0^{2\pi}d\phi'\,\frac{\partial}{\partial\tau'}\left[b^2+(\tau'-8\mu\ln\psi+\rho\cos\phi'+8\mu\ln\rho)^2\right]^{-5/2}+o(\psi^{-2}) \qquad (6.20)$$

as $\psi\to\infty$, where the leading ψ^{-2} behavior arises in $\partial g_{xx}^{(2)}/\partial\tau$, while $\partial g_{xy}^{(2)}/\partial\tau$ decreases as ψ^{-3} for large ψ.

Note also the complicated dependence of $Q_0(\tau,\psi,\phi)$ on the black-hole masses, through the dimensionless quantity μ/b. This differs from the quadratic dependence (news function $\propto M_1M_2$) found by other authors for encounters so distant as to be tractable by "fast-motion" perturbation theory based on Minkowski space (Kovács and Thorne[22] and Peters[23]). Once again, this difference emphasizes that the methods used here can deal with much closer high-speed encounters—generating much more radiation—than are amenable to other perturbation approaches. The validity of the "fast-motion" methods is limited by their requirement that the perturbations of flat space be everywhere weak. For an encounter of equal masses M (say) at large γ, viewed in a center-of-mass frame, the condition becomes $M\gamma^2\ll$ impact parameter, found by considering the metric component g_{tt}. But the calculations of this section are still valid when the impact parameter is comparable to $M\gamma^2$.

Both types of method should give an accurate description of the beamed radiation when we take $b\gg1$. Thus our results should match as $b\to\infty$ onto the $\gamma\to\infty$ results of the other methods. In this limit we can actually carry out the integrals involved in the leading behavior of $Q_0(\tau,\psi,\phi)$. For large b, the main contribution to the integrals (6.19a) and (6.19b) arises from X and Y values of order b. Then the "delay" term $4\mu\ln(X^2+Y^2)$ becomes a small correction when compared with the terms $X\psi\cos\phi$ and $Y\psi\sin\phi$. By transforming to integration variables Xb^{-1}, Yb^{-1}, and expanding out the small "delay" corrections in a Taylor series, we find the leading behavior

$$Q_0(\tau,\psi,\phi)=\frac{6\mu^2e^{-2i\phi}}{\pi b^2}\int_{-\infty}^{\infty}\int_{-\infty}^{\infty}dX\,dY(X+iY+1)^2 \times\ln(X^2+Y^2)\frac{\partial}{\partial(\tau/b)}[(X+1)^2+Y^2+(\tau b^{-1}+X\psi\cos\phi+Y\psi\sin\phi)^2]^{-5/2}+o(b^{-2}) \tag{6.21}$$

as $b\to\infty$. This already exhibits the quadratic factor $(\mu/b)^2$ which sets the order of magnitude of the news function, and also shows that the characteristic timescale of the radiation is provided by $b=$ (impact parameter)$/\gamma$ in this regime.

The integral in Eq. (6.21) can either be evaluated directly, or computed with the help of the Green's function techniques in weakly curved spacetime, set up by Thorne and Kovács.[24] The result is

$$\begin{aligned}Q_0(\tau,\psi,\phi)=&\frac{8\mu^2e^{-2i\phi}}{(\psi^2+1)(\tau^2+b^2)^{3/2}[4\psi^2\tau^2+4b\psi\cos\phi(1-\psi^2)\tau+b^2(1+2\psi^2-4\psi^2\cos^2\phi+\psi^4)]^2}\\
&\times\{(\psi^2+1)\{8\psi^2(\psi^2-1)(2\cos^2\phi-1)\tau^5+8b\psi\cos\phi[-\psi^4+(4\cos^2\phi-2)\psi^2-1]\tau^4\\
&\quad+2b^2(\psi^2-1)[\psi^4+(8\cos^2\phi-4)\psi^2+1]\tau^3+4b^3\psi\cos\phi[-3\psi^4+(12\cos^2\phi-4)\psi^2-3]\tau^2\\
&\quad+b^4(\psi^2-1)[3\psi^4-(12\cos^2\phi+2)\psi^2+3]\tau+2b^5\psi\cos\phi[\psi^4+(4\cos^2\phi-6)\psi^2+1]\}\\
&\pm2(\tau^2+b^2)^{3/2}\{4\psi^2(\psi^4+1)(1-2\cos^2\phi)\tau^2+4b\psi\cos\phi(\psi^2-1)[\psi^4+4(\sin^2\phi)\psi^2+1]\tau\\
&\quad+b^2[-\psi^8+(4\cos^2\phi-2)\psi^6+(16\cos^2\phi\sin^2\phi-2)\psi^4+(4\cos^2\phi-2)\psi^2-1]\}\\
&+4i(\psi^2+1)\psi\sin\phi(\tau^2+b^2)\{4\psi\cos\phi(\psi^2-1)\tau^3+2b[-\psi^4+4(\cos^2\phi)\psi^2-1]\tau^2+b^3[-\psi^4+(4\cos^2\phi-2)\psi^2-1]\}\\
&\pm8i\psi\sin\phi(\tau^2+b^2)^{3/2}\{-2\psi\cos\phi(\psi^4+1)\tau^2+b(\psi^2-1)[\psi^4+(2-4\cos^2\phi)\psi^2+1]\tau\\
&\quad+b^2\psi\cos\phi[\psi^4+(2-4\cos^2\phi)\psi^2+1]\}\}\\
&+o(b^{-2})\end{aligned} \tag{6.22}$$

as $b\to\infty$. The upper sign applies when $\tau<b\psi\cos\phi$, and the lower when $\tau>b\psi\cos\phi$. The discontinuous behavior given by Eq. (6.22) at $\tau=b\psi\cos\phi$ has appeared as a result of fixing attention on τ values comparable with b, before letting $b\to\infty$. For any particular large finite b, the news function will be continuous near $\tau=b\psi\cos\phi$, but will vary there over timescales short compared to b, which cannot be seen in the expansion (6.22). These more rapid variations are unimportant by comparison with the behavior in Eq. (6.22), in the sense that they carry a negligible fraction of the total energy radiated, in the limit $b\to\infty$.

When the black-hole masses are unequal, these calculations of the radiation field near the axis must again be modified slightly; near the forward direction γ should be replaced by γ_1, and near the backward direction γ should be replaced by γ_2. Thus

$$Q_0(\tau,\psi,\phi)=\lim_{\gamma\to\infty}c_\tau(\tau,\theta=\psi/\gamma_1,\phi)$$

will have the same functional form if we scale the impact parameter $=b\gamma_1$, while working in a center-of-mass frame.

If one is only interested in the dominant beamed part of the radiation generated by a high-speed encounter, there is no need to restrict attention to black holes. The expressions for the leading radiation field should still be accurate when the proper radii R_1, R_2 of the two bodies satisfy $R_1 \ll M_1(\gamma_1)^2$, $R_2\ll M_2(\gamma_2)^2$, while the impact parameter is comparable to (or larger than) $M_1(\gamma_1)^2$ and $M_2(\gamma_2)^2$. This is simply because the detailed structure of such bodies is not apparent on the length scales of $O(\gamma)$ in the x and y directions, and of $O(1)$ in the z direction, appropriate to the far-field curved shocks where the radiation is generated.

VII. CONCLUSION

We have seen in this paper how certain parts of any spacetime formed by the high-speed collision or encounter of two black holes with comparable masses can be described using perturbation methods. When the impact parameter is of order $\mu\gamma$ or larger, so that we have a fairly distant encounter, essentially all of the spacetime geometry can be analyzed by perturbation theory, as in Sec. VI. But even when the impact parameter is comparable to the energy μ, so that there is a highly nonlinear collision, useful information about the

spacetime can be extracted from a description of the shock regions which form the boundary of the strong-field interaction zone. In the special case of an axisymmetric collision, with zero impact parameter, these shock regions have been analyzed in Secs. III, IV, and V.

In the author's opinion, the most significant outcome of this treatment has been the calculation of the gravitational radiation emitted near the forward and backward directions, found by considering the evolution of the far-field shocks after they have distorted each other during their interaction. By this means we have been able to find beamed bremsstrahlung radiation in a regime not explored by previous authors, where the impact parameter is of order $\mu\gamma$. Such an encounter is sufficiently close that it generates radiation of the typical strong-field power/solid angle c^5G^{-1}, lasting a time of $O(\mu)$, which emerges in a beam at angles of $O(\gamma^{-1})$ from the direction of motion. This radiation is described by Eqs. (6.17), (6.19a), and (6.19b). Thus the present treatment differs from most other perturbation calculations of gravitational wave generation, which work with asymptotic expansions valid only in the limit that the radiation becomes weak.

Similar techniques have been applied to find the detailed structure of the radiation on angular scales of $O(\gamma^{-1})$ near the direction of motion, when the impact parameter is of order μ and the black holes undergo a close encounter or a collision. The leading term in the asymptotic expansion for such radiation is given by Eq. (5.24), and this news function is depicted in Fig. 7. Again the radiation has the intensity characteristic of fully nonlinear gravitational interactions, but it does not appear to be beamed. Instead, the news function tends to a limiting shape at angles θ satisfying $\gamma^{-1} \ll \sin\theta \ll 1$; this should allow the radiation near the axis to merge into a much smoother radiation pattern spread all over the celestial sphere. In particular, the limiting news function of Eq. (5.28) should be precisely the news function at $\theta = 0$ produced by a collision at the speed of light. Thus we have found part of a strong-field news function while using only perturbation methods. Clearly, it is only the very special nature of the collision problem at large γ which has made this possible. This has allowed us to calculate the dominant radiation near the axis by examining the collision of the Coulomb far fields of the two black holes. As suggested in Sec. V, one could go on from here to build up more information about the angular structure of the full $\gamma = \infty$ news function, by solving inhomogeneous wave equations in the far-field curved shocks and finding higher-order terms in the expansion (5.25), before matching out to the expansion (5.29). At each higher order, the calculation would dig further and further into the nonlinear details of the strong-field interaction region, allowing for more powers of r^{-1} in the incoming fields. If carried to completion, this process would enable us to calculate the true efficiency for the conversion of incoming energy into gravitational waves during an axisymmetric collision at the speed of light. At present, our only guide as to that true efficiency is provided by the limiting news function, which would give an efficiency of 24.8% if it were part of an isotropic radiation pattern.

Finally, the importance of a search for exact solutions representing high-speed black-hole collisions should be emphasized. If any black-hole collision spacetime can be found analytically, it will be the axisymmetric solution where the black holes approach one another at the speed of light with zero impact parameter. Together with the numerical calculations of black-hole collisions by Smarr[25] and Eppley,[26] such a solution would be of considerable value in testing the prevalent ideas on gravitational collapse with formation of event horizons and the emission of gravitational radiation.

ACKNOWLEDGMENTS

I wish to thank G. E. Curtis, S. W. Hawking, R. Penrose, and L. Smarr for helpful conversations relating to the interactions of black holes. I am also grateful to S. J. Kovács for pointing out an error in an earlier version of this paper, and to J. M. Stewart for assistance with algebraic computing.

---

[1]We shall normally use units in which $c = G = 1$.

[2]P. C. Aichelburg and R. U. Sexl, Gen. Relativ. Gravit. 2, 303 (1971).

[3]J. Ehlers and W. Kundt, in *Gravitation*, edited by L. Witten (Wiley, New York, 1962).

[4]S. W. Hawking and G. F. R. Ellis, *The Large Scale Structure of Spacetime* (Cambridge Univ. Press, New York, 1973), Chap. 6.

[5]R. Penrose, seminar at Cambridge University, 1974 (unpublished).

[6]G. E. Curtis, D. Phil. thesis, Oxford University, 1975 (unpublished).

[7]R. Penrose, in *General Relativity*, papers in honor of J. L. Synge, edited by L. O'Raifeartaigh (Oxford Univ.

Press, Oxford, England, 1972).
[8]F. A. E. Pirani, Proc. R. Soc. London A252, 96 (1959).
[9]A. Einstein and N. Rosen, J. Franklin Inst. 223, 43 (1937).
[10]A. G. Mackie, *Boundary Value Problems* (Oliver and Boyd, London, England, 1965).
[11]P. Szekeres, J. Math. Phys. 13, 286 (1972).
[12]M. Abramowitz and I. A. Stegun, *Handbook of Mathematical Functions* (Dover, New York, 1965), Chap. 17 and p. 560.
[13]Reference 12, Eqs. (8.1.2) and (15.3.10).
[14]R. A. Matzner and Y. Nutku, Proc. R. Soc. London A336, 285 (1974).
[15]R. Penrose, in A. R. L. Technical Documentary Report No. 63-56, 1963 (unpublished).
[16]The characteristic initial-value problem for the flat-space wave equation with data on null planes is also discussed in F. G. Friedlander, *The Wave Equation on a Curved Spacetime* (Cambridge Univ. Press, New York, 1975). Unfortunately there is a mistake in the integral representation of Eq. (5.4.28); the denominators $(t-\rho_1)$ and $(t-\rho_2)$ in the first and second lines should be replaced by $(t-X_1)$ and $(t+X_1)$, respectively.
[17]H. Bondi, M. G. J. van der Burg, and A. W. K. Metzner, Proc. R. Soc. London A269, 21 (1962).
[18]L. Smarr, Phys. Rev. D 15, 2069 (1977).
[19]P. D. D'Eath, Phys. Rev. D 11, 1387 (1975).
[20]R. K. Sachs, Proc. R. Soc. London A270, 103 (1962).
[21]P. L. Chrzanowski, R. A. Matzner, V. D. Sandberg, and M. P. Ryan, Phys. Rev. D 14, 317 (1976).
[22]S. J. Kovács and K. S. Thorne, Astrophys. J. 217, 252 (1977).
[23]P. C. Peters, Phys. Rev. D 1, 1559 (1970).
[24]K. S. Thorne and S. J. Kovács, Astrophys. J. 200, 245 (1975).
[25]L. Smarr, Ph.D. thesis, University of Texas at Austin, 1975 (unpublished).
[26]K. R. Eppley, Ph.D. thesis, Princeton University, 1975 (unpublished).

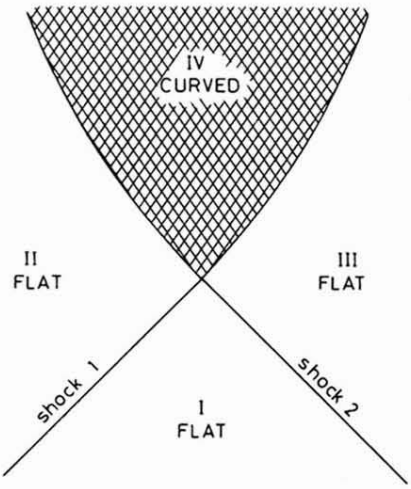

FIG. 1. Schematic spacetime diagram for a collision of two black holes approaching at the speed of light. Before the collision, the spacetime curvature due to black hole 1 resides on a null hyperplane, denoted by shock 1, which separates two regions I and II of flat spacetime. Similarly there is a null shock 2 produced by black hole 2, which separates region I from another flat region III. At the collision, the null generators of each shock acquire shear and begin to converge; thereafter the shock surfaces are curved. Spacetime curvature develops in the region IV to the future of the collision.

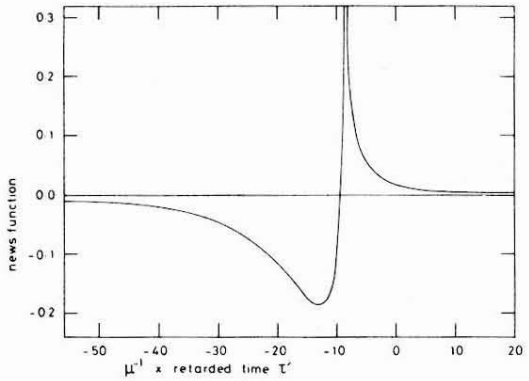

FIG. 10. The news function showing the gravitational radiation produced by a high-speed axisymmetric collision, at angles θ satisfying $\gamma^{-1} \ll \theta \ll 1$. This is found by taking the limit as $\psi \to \infty$ of the new function shown in Fig. 7. The peak has become infinitely high in this limit, with a logarithmic singularity; the time interval between trough and peak is approximately 4.5μ.

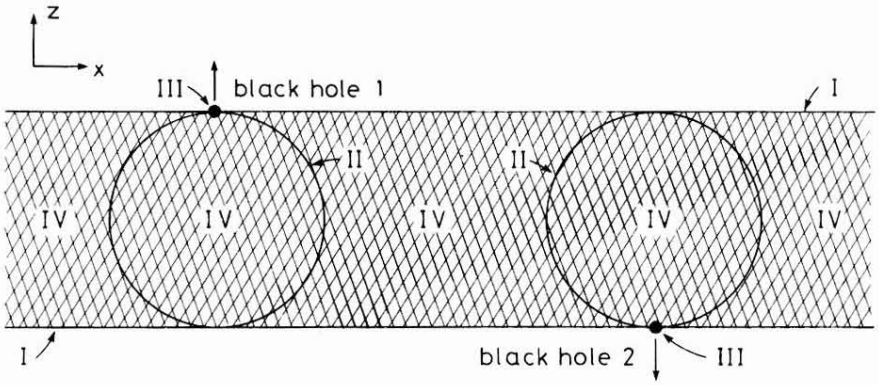

FIG. 11. A high-speed encounter with impact parameter $b\gamma$ leads to a variety of types of gravitational radiation, generated in different parts of the spacetime. The various different regions are seen here in the plane of motion of the black holes, at a time $\frac{1}{4}b\gamma$ after the shocks have met. The dominant beamed part of the radiation is produced in the far-field shocks (I), which are just beginning to evolve after their collision. Weak radiation is generated at distances of $O(1)$ from each black hole as it passes through the other shock, and propagates out in all directions (II). High-frequency beamed radiation generated at distances of $O(\gamma^{-1})$ from each black hole is still close to the holes, in the regions III. Region IV contains weak low-frequency radiation, left in the wake of the shocks.

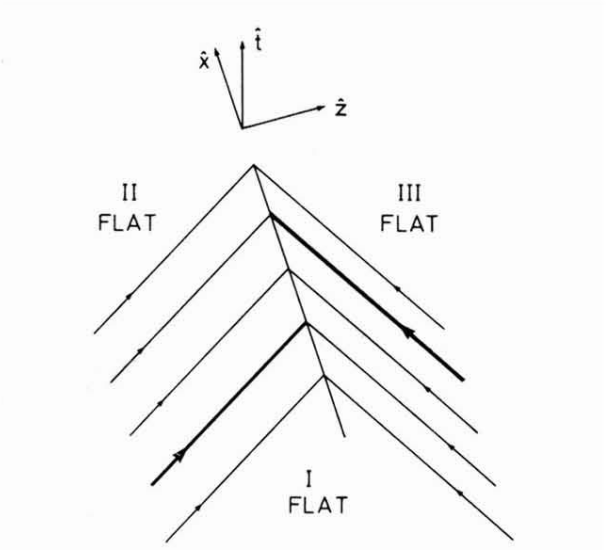

FIG. 2. The two null shocks are shown approaching before the collision; one spatial dimension has been suppressed. The incoming shock 1 lies on the surface $\{\hat{z}=\hat{t}\}$ separating the flat regions I and II, while shock 2 lies on the surface $\{\hat{z}=-\hat{t}\}$ between the flat regions I and III. Some null generators have been drawn on each null surface; the heavy lines show the null world lines at the center of the shocks—these are all that remain of the black holes after boosting to the speed of light. In the collision drawn here, the central world lines do not intersect, and the spacetime is nonaxisymmetric.

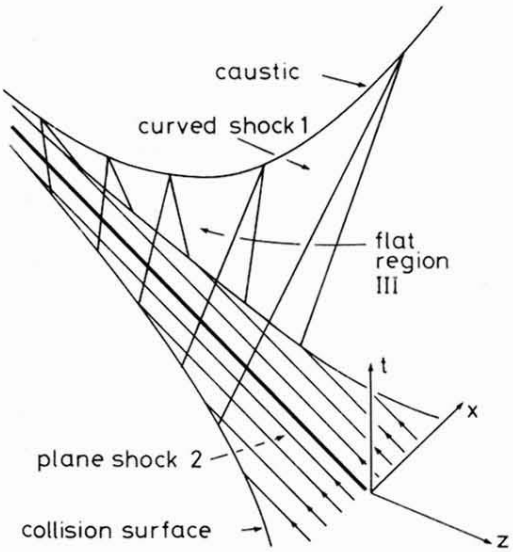

FIG. 3. In an axisymmetric collision at the speed of light, the region III of flat spacetime is bounded by the plane shock 2 and the curved shock 1. One spatial dimension has been suppressed, and the coordinates are Minkowskian for region III. Some null generators of shock 2 have been drawn, including the heavy line at the center of the shock. Each null generator of shock 2 eventually meets shock 1 on the collision surface, which is two-dimensional, spacelike, and noncompact. In the diagram, the collision surface appears as a pair of lines. The null generators of the curved shock 1 emerge through the collision surface, and come to a focus on the caustic region at the top of the diagram. The caustic region is a spacelike line which becomes asymptotically null at both ends, and lies on the axis of symmetry.

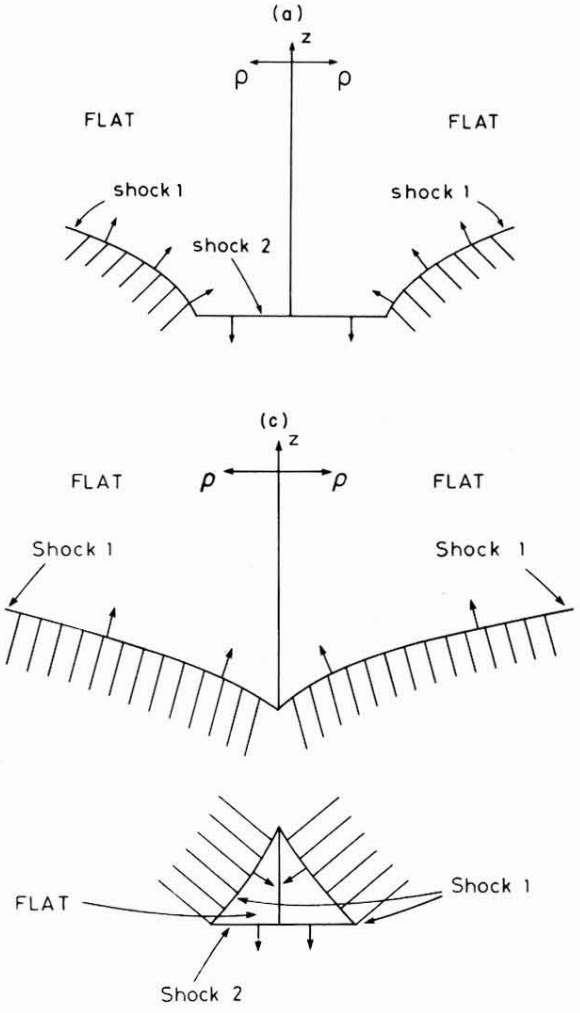

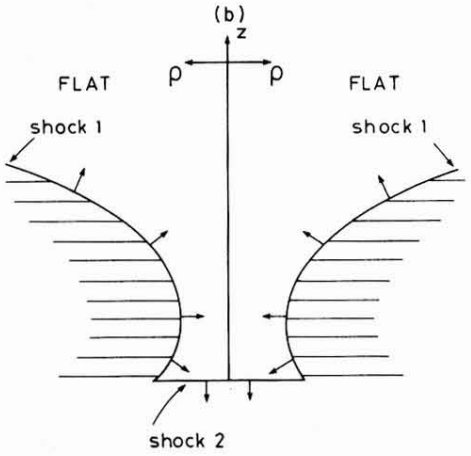

FIG. 4. (a), (b), and (c) The curved shock 1 is seen at three successive times t as it moves at the speed of light into the flat region III. The diagrams show the instantaneous shock front in a neighborhood of the symmetry axis; z measures distance along the axis, and ρ measures distance away from the axis in the Minkowskian region III. Also shown is the plane front of shock 2, which moves down the axis at the speed of light. The arrows on the shocks give their direction of motion. At the earliest time (a) all of shock 1 moves in the positive z direction; the null generators which have been deflected by the largest angle are those which were closest to the axis at the collision with shock 2—further out from the axis the shock front has a logarithmic shape. Later (b) shock 2 has moved down to reveal a part of shock 1 which moves in the negative z direction, due to the very strong deflection produced near the axis. Still later (c), shock 1 has reached the axis; one part of shock 1 moves upward, and the other downward. Shock 1 meets the axis at the caustic region, which travels along the axis at more than the speed of light.

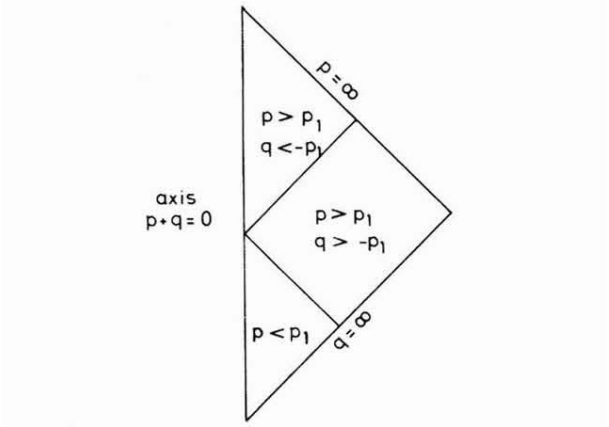

FIG. 5. The domain of the coordinates p, q, used in describing the caustic region. The domain is bounded by the axis $\{p+q=0\}$ and the two "null infinities" $\{q=\infty\}$, $\{p=\infty\}$; waves are fed into the caustic region at $q=\infty$ by shock 1, and then interact with themselves before emerging in another shock behind the caustic region, at $p=\infty$. Also shown are the three domains appearing in Eq. (4.19).

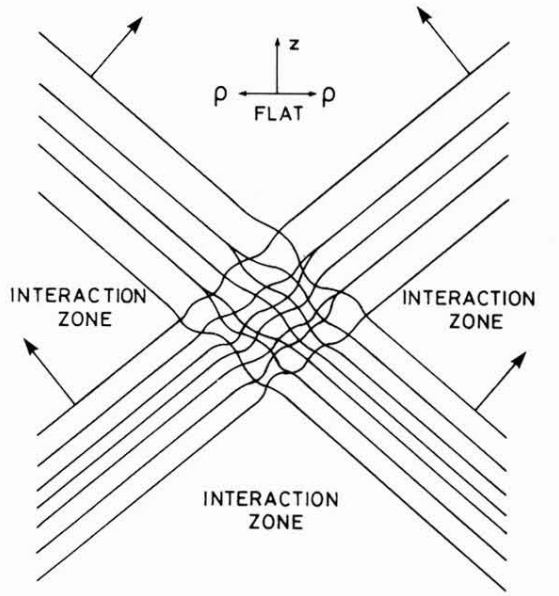

FIG. 6. Schematic diagram showing the caustic region produced as curved shock 1 crosses over itself near the symmetry axis, while moving upward into the flat spacetime region III. Distance along the axis is given by z, while ρ measures distance away from the axis in this representation of the instantaneous shock profile. The incoming shock 1 is shown in the top half of the diagram, separating the flat region III from the interaction zone IV, where the spacetime is strongly curved. As it moves in the arrowed direction, it undergoes a wavelike self-interaction in the center of the diagram. The shock re-forms and continues to move in the arrowed direction after its self-interaction, at the bottom of the diagram; however, the shock profile has been altered in the caustic region.

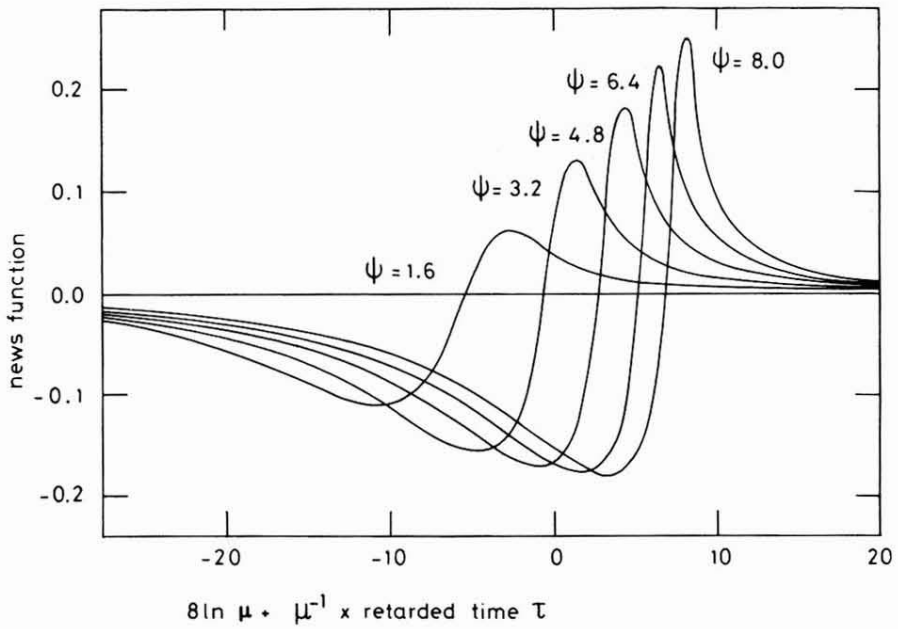

FIG. 7. The dominant news function, giving the amount of gravitational radiation emitted in a high-speed axisymmetric collision, at angles $\theta = \psi\gamma^{-1}$ close to the axis. Plotted horizontally is retarded time τ, measured in units of the energy μ of one incoming black hole. The square of the news function gives $(4\pi) \times$ power radiated/solid angle. The characteristic angular frequencies associated with the time interval between the minimum and maximum of the news function lie roughly in the range $0.3\,\mu^{-1}$–$0.6\,\mu^{-1}$, although lower frequencies are also important. As ψ is increased, the higher frequencies should gain in amplitude, since the time interval from minimum and maximum decreases and since the maximum grows into a higher and higher spike.

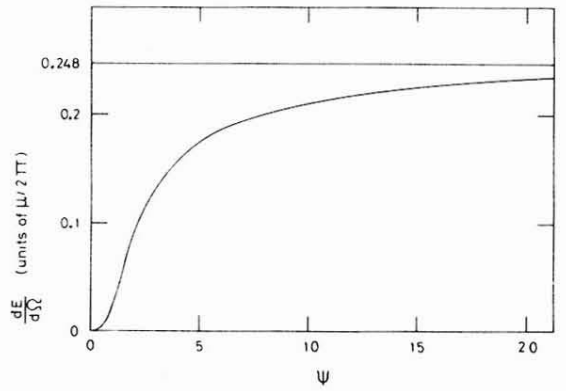

FIG. 8. Time-integrated power/solid angle in gravitational waves produced by a high-speed axisymmetric collision, at angles $\theta = \psi\gamma^{-1}$ close to the axis. On the vertical axis, energy/solid angle is measured in units of $\mu/2\pi$ in order to show the efficiency of the process in converting collision energy into gravitational waves; the units give the efficiency which the collision would have if the radiation were distributed isotropically with the news function seen at angle $\psi\gamma^{-1}$. At angles θ satisfying $\gamma^{-1} \ll \theta \ll 1$, $dE/d\Omega$ will be close to the limiting value $0.248\ \mu/2\pi$. However, $dE/d\Omega$ may be different for larger values of θ.

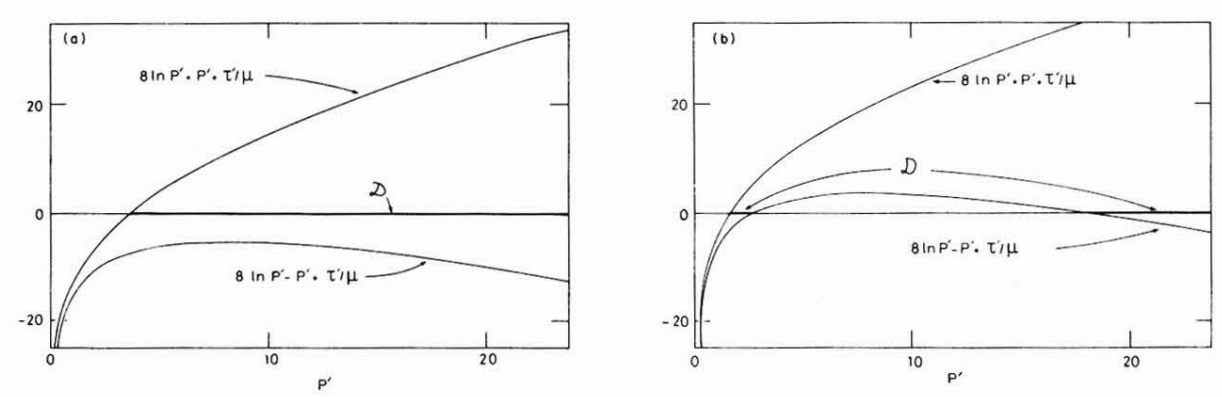

FIG. 9. (a) and (b) The domain $\mathfrak{D}$ of integration for Eq. (5.28), consisting of those numbers $P' > 0$ such that $8 \ln P' - P' + \tau'/\mu < 0 < 8 \ln P' + P' + \tau'/\mu$. In (a), $\tau'/\mu = -14.0 < 8 - 8 \ln 8$, so that $\mathfrak{D}$ is one connected region. In (b), $\tau'/\mu = -5.0 > 8 - 8 \ln 8$, and $\mathfrak{D}$ is in two disjoint pieces.